Journal of Medicinal Chemistry

Article

pubs.acs.org/jmc

Optimization of Benzodiazepinones as Selective Inhibitors of the X-Linked Inhibitor of Apoptosis Protein (XIAP) Second Baculovirus IAP Repeat (BIR2) Domain

Robert F. Kester,*[,†] Andrew F. Donnell,[†] Yan Lou,[†] Stacy W. Remiszewski,[†] Louis J. Lombardo,[†] Shaoqing Chen,[†] Nam T. Le,[†] Jennifer Lo,[†] John A. Moliterni,[†] Xiaochun Han,[†] J. Heather Hogg,[†] Weiling Liang,[†] Christophe Michoud,[†] Kenneth C. Rupert,[†] Steven Mischke,[†] Kang Le,[†] Martin Weisel,[†] Cheryl A. Janson,[‡] Christine M. Lukacs,[‡] Adrian J. Fretland,[§] Kyoungja Hong,[∥] Ann Polonskaia,[∥] Lin Gao,[‡] Shirley Li,[‡] Dave S. Solis,[‡] Doug Aguilar,[‡] Christine Tardell,[∥] Mark Dvorozniak,[∥] Shahid Tannu,[∥] Edmund C. Lee,[∥] Andy D. Schutt,[∥] and Barry Goggin[∥]

[†]Departments of Discovery Chemistry, [‡]Discovery Technologies, [§]Non-clinical Safety, Early ADME, and [∥]Discovery Oncology, Hoffmann-La Roche Inc., 340 Kingsland Street, Nutley, New Jersey 07110, United States

Supporting Information

ABSTRACT: The IAPs are key regulators of the apoptotic pathways and are commonly overexpressed in many cancer cells. IAPs contain one to three BIR domains that are crucial for their inhibitory function. The pro-survival properties of XIAP come from binding of the BIR domains to the pro-apoptotic caspases. The BIR3 domain of XIAP binds and inhibits caspase 9, while the BIR2 domain binds and inhibits the terminal caspases 3 and 7. While XIAP BIR3 inhibitors have previously been reported, they also inhibit cIAP1/2 and promote the release of TNFα, potentially limiting their therapeutic utility. This paper will focus on the optimization of selective XIAP BIR2 inhibitors leading to the discovery of highly potent benzodiazepinone **36** (IC_{50} = 45 nM), which has high levels of selectivity over XIAP BIR3 and cIAP1 BIR2/3 and shows efficacy in a xenograft pharmacodynamic model monitoring caspase activity while not promoting the release of TNFα in vitro.

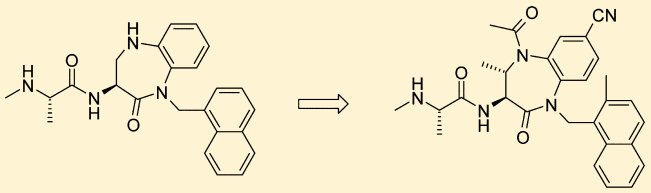

INTRODUCTION

A defining characteristic of tumor growth is the uncontrolled proliferation of cancer cells. In addition to abundant cell proliferation signals, faulty apoptotic mechanisms may contribute to the rapid expansion of the tumor cell population.[1] The final effectors of apoptosis are the cellular caspases, including the gatekeeper caspases 8 and 9 and the terminal caspases 3 and 7. The inhibitor of apoptosis proteins (IAPs), of which the X-linked inhibitor of apoptosis protein (XIAP) is a member, represent the final barrier to apoptosis by acting as regulators of the caspase activity, inhibiting their action and preventing the destruction of the cell.[2] In recent years, research has shown that there is a correlation between XIAP expression and patient outcomes in certain cancers. In adult and childhood de novo acute myeloid leukemia (AML), increased XIAP expression correlates to decreased survival times when compared to patients with low XIAP levels.[3] More recently, it has been shown that XIAP expression levels correlate with tumor stage and degree of progression (metastatic disease) in melanoma.[4] In renal cell carcinoma, the XIAP expression levels correlated to the grade of RCC and predicted a worse prognosis.[5] Small molecule inhibitors of XIAP that restore apoptosis to tumor cells might therefore be an effective treatment for cancers where XIAP is overexpressed.

The members of the IAP family are characterized by the presence of one to three baculovirus IAP repeat (BIR) domains, each of which contains an approximately 80 amino acid zinc binding region.[6] XIAP, the most well-characterized IAP member, is a 57 kDa protein that contains three BIR domains (BIR1−3) and a really interesting new gene (RING) domain which confers ubiquitin protein ligase (E3) activity. Other IAP family members, such as the closely related cellular inhibitor of apoptosis proteins (cIAP1 and cIAP2), also contain multiple BIR domains. XIAP is believed to be the only IAP that binds and directly inhibits the caspases via its BIR domains.[2]

There are two main pathways to initiate caspase-mediated cell death, the intrinsic and extrinsic pathways. The intrinsic pathway is activated in response to intracellular damage, such as that caused by chemotherapeutic agents, and leads to activation of caspase 9 via the apoptosome.[7] On the other hand, the extrinsic pathway is activated by the binding of death ligands,

Received: May 15, 2013

   dx.doi.org/10.1021/jm400732v | *J. Med. Chem.* XXXX, XXX, XXX−XXX

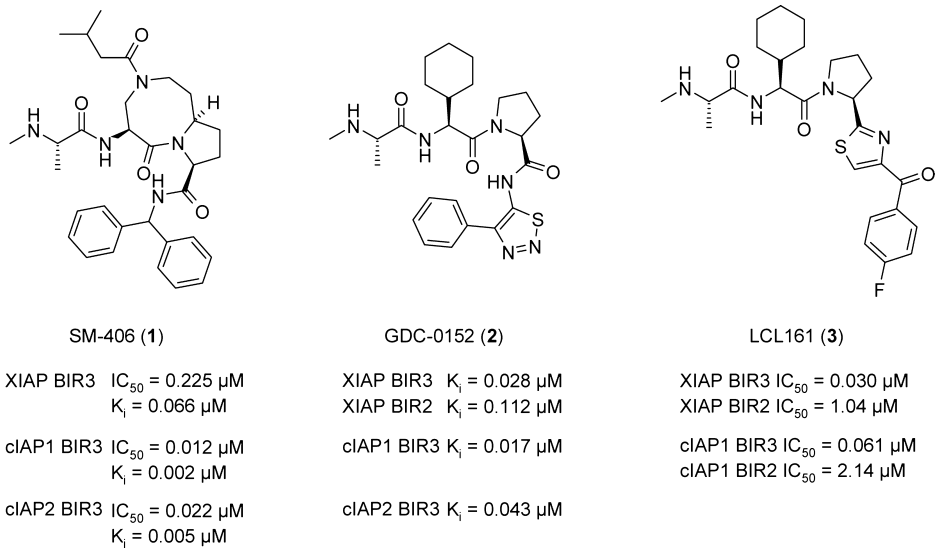

Figure 1. IAP inhibitors. Values for **1** and **2** are from refs 13 and 14, respectively. Values for **3** were generated in-house.

such as FasL, TNF-related apoptosis-inducing ligand (TRAIL), and TNFα, to their respective death receptors, Fas, DR4 or DR5, and TNFR1, resulting in the activation of caspase 8.[8] Regardless of which signaling pathway is activated, both caspase 8 and 9 lead to activation of the terminal caspases 3 and 7.[9] XIAP is able to inhibit both the intrinsic and extrinsic pathways through the binding of the BIR3 domain to caspase 9 and the BIR2 domain to the terminal caspases 3 and 7.[10]

The inhibition of the caspases by XIAP can be antagonized by the endogenous mitochondrial protein Smac/DIABLO (second mitochondria-derived activator of caspases/direct IAP-binding protein with low p*I*) which is secreted from the mitochondria in response to pro-apoptotic stimuli.[11] The function of Smac/DIABLO is dependent on a four amino acid sequence (AVPI) at its *N*-terminus that binds to the BIR3 domain of XIAP and disrupts its interaction with the caspases.[12] This AVPI sequence served as the basis for much of the initial work in the XIAP antagonist field and resulted in a few small molecule IAP inhibitors[13] that have entered the clinic. Structure-based design efforts starting from the AVPI sequence by Shaomeng Wang's group at the University of Michigan identified SM-406[14] (**1**, Figure 1), which was taken into phase I trials in partnership with Ascenta. In separate peptidomimetic approaches, Genentech identified GDC-0152[15] (**2**) while Novartis identified LCL161[16] (**3**) as potent IAP inhibitors which have entered clinical trials.[17] The data for these Smac-mimetic compounds indicate these compounds are pan-IAP inhibitors with a preference for BIR3 binding. In addition to binding to XIAP, they also bind to cIAP1 and cIAP2. This results in the autoubiquitination and degradation of the cIAPs and activates the noncanonical NF-κB pathway, leading to the production of TNFα.[18] The pro-apoptotic effect of these compounds is potentially mediated through increased TNFα signaling, and it represents a potential liability due to the increase in TNFα levels. It was expected that selective targeting of the BIR2 domain of XIAP would disrupt the interaction with the terminal caspases 3 and 7 and promote apoptosis in a manner mechanistically distinct from the pan-IAP inhibitors with a preference for BIR3 binding, by not binding to cIAP1/2, and might result in different PD properties. A recent paper[19] from the Sanford–Burnham Institute described efforts leading to a submicrolar monovalent Smac-mimetic with modest selectivity (up to 7:1) for XIAP BIR2 versus XIAP BIR3 that could serve as a probe compound to investigate the effects of selective XIAP BIR2 inhibitors. In addition to these monomeric compounds, there has been work focused on dimeric Smac mimetics[13] that may bind BIR2 as well as BIR3, however, their overall activity may be different than a selective BIR2 monomeric compound.

In a previous paper, we described the medicinal chemistry efforts leading to benzoxazepinone **4**[20] (Figure 2), which served

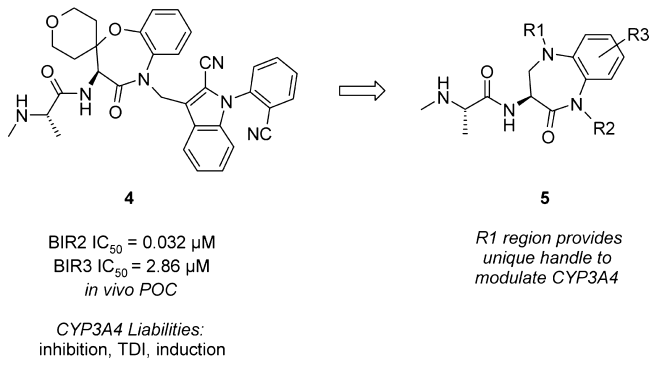

Figure 2. Benzoxazepinone proof-of-concept compound **4** and plan to address CYP3A4-related liabilities by exploration of benzodiazepinone scaffold **5**.

as an in vivo proof of concept molecule[21] and demonstrated that selective BIR2 XIAP inhibitors could potentiate the effects of a DR5 mAB in inducing apoptosis without causing the release of TNFα. However, this molecule was not adequate as a clinical lead due to CYP3A4-related in vitro safety issues. It exhibited strong CYP3A4 inhibition (IC_{50} = 1.8 μM) and time-dependent inhibition (TDI) of CYP3A4 (K_I = 1.0 μM, k_{inact} = 0.043 min^{-1}, k_{inact}/K_I = 0.043 L/min/μmol) and displayed unacceptable CYP3A4 induction levels (CYP3A4 mRNA >40% of control at 10 μM **4**). In a parallel effort, we were investigating the benzodiazepinone series of compounds **5** (Figure 2). Due to similarities between these scaffolds, we anticipated the SAR would be transferrable to this series, and we planned to draw upon lessons from the benzoxazepinones

dx.doi.org/10.1021/jm400732v | J. Med. Chem. XXXX, XXX, XXX–XXX

Scheme 1. Synthesis of Unsubstituted and *N*-Acyl Analogues[a]

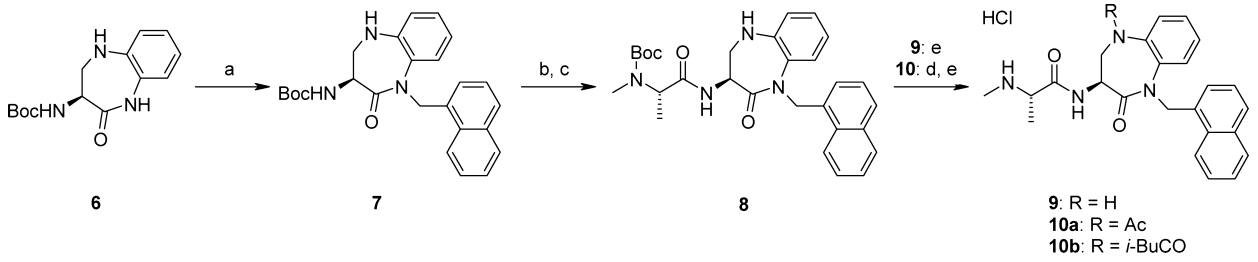

[a]Reagents and conditions: (a) LiHMDS, THF, −78 °C; 1-(bromomethyl)naphthalene, 78%; (b) HCl, 1,4-diox, rt, 99%; (c) Boc-*N*-methyl-L-alanine, HBPyU, HOBt, *i*-Pr_2NEt, DMF, 0 °C to rt, 80%; (d) for **10a**, AcCl; for **10b**, *i*-BuCOCl, Et_3N, CH_2Cl_2, rt, 37−82%; (e) HCl, 1,4-diox, rt, 70%−quant.

Scheme 2. Synthesis of *N*-Alkyl Analogues[a]

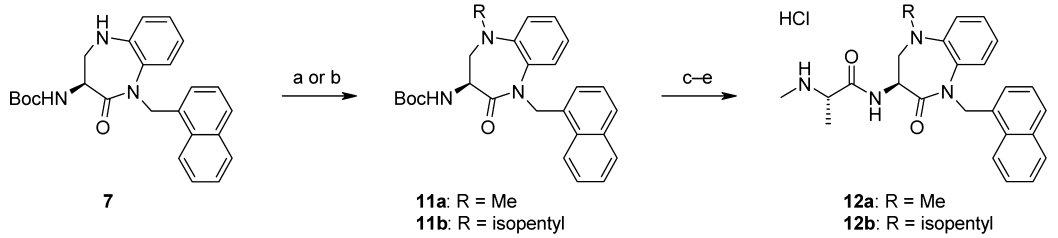

[a]Reagents and conditions: (a) MeI, K_2CO_3, DMF, rt, 30%; (b) isovaleraldehyde, $NaBH(OAc)_3$, CH_2Cl_2, rt, 85%; (c) HCl, 1,4-diox, rt, quant; (d) Boc-*N*-methyl-L-alanine, HBPyU, HOBt, *i*-Pr_2NEt, DMF, 0 °C to rt, 81%; (e) HCl, 1,4-diox, rt, quant.

to guide our exploration and optimization of the benzodiazepinone scaffold. It was also expected that there would be subtle differences between the two series due to the additional nitrogen in the core ring system which could serve as a handle for substitution. Our plan focused on the iterative exploration of the R1, R2, and R3 regions of **5** as defined in Figure 2. In particular, the R1 region provided a unique vector for optimization that was not available in the benzoxazepinones. From an analysis of the X-ray crystal structure of the benzoxazepinones, it was apparent that the nitrogen atom in the R1 region would be pointing into a solvent exposed area, and we believed it might be possible to use this nitrogen as a handle to introduce groups that could modulate the CYP3A4 inhibition and TDI liability. In conjunction with this, we planned to re-examine the R2 and R3 regions with a goal of minimizing CYP3A4 issues. In earlier work (data not shown), it was confirmed that the *N*-methyl-L-alanine chain was optimal. This paper will detail the optimization of the benzodiazepinone series leading to the identification of compound **36**, a potential clinical candidate.

RESULTS AND DISCUSSION

The starting point for our investigation was based on an early analogue in the benzoxazepinone series with a naphthyl group in the R2 region. Our SAR exploration began with a small set of substituents in the R1 region to determine whether substitution is tolerated and to identify the optimal linker type, either acyl or alkyl. The unsubstituted benzodiazepinone **9** was prepared in four steps according to the synthesis outlined in Scheme 1. BOC-protected amino benzodiazepinone **6**[22] was deprotonated with 1.1 equiv of lithium hexamethyldisilazide, and the amide nitrogen was selectively alkylated with 1-(bromomethyl)-naphthalene to afford the naphthyl-substituted analogue **7**. The alanine moiety was then installed by deprotection of the amine and coupling with BOC-*N*-methyl-L-alanine to yield **8**, which was deprotected to provide **9**. Acylated compounds **10a−b** were prepared via treatment of **8** with the corresponding acid chloride in the presence of a base, then removal of the BOC group. The final compounds were obtained and tested as the hydrochloride salts.

The *N*-alkyl analogues were synthesized in four steps from **7** as detailed in Scheme 2. Compound **7** was either alkylated with methyl iodide in the presence of potassium carbonate to produce **11a** or treated with isovaleraldehyde under reductive amination conditions to produce **11b**. The deprotection, amide coupling, deprotection sequence provided compounds **12a** and **12b** as the hydrochloride salts.

The ability of the these compounds to inhibit XIAP BIR2 and BIR3 was determined using a TR-FRET assay measuring the displacement of a Smac derivative from either the BIR2 or BIR3 domain of XIAP. The results of this initial SAR exploration of the nitrogen substituents are displayed in Table 1. The alkyl substituted compounds **12a** and **12b** were roughly of equal potency at BIR2 to the unsubstituted compound **9**. When the amide compounds **10a** and **10b** were tested, they showed approximately a 4-fold increase in potency over the corresponding alkyl compounds, **12a** and **12b**, while maintaining excellent selectivity over the BIR3 domain (>54.8 μM). This confirms that the R1 region is amenable to modification and supported our plan to explore it more exhaustively with the goal of modulating the CYP3A4 inhibition. Before continuing that effort, however, we explored the SAR in the other regions of the molecule to provide a starting point with greater BIR2 potency.

Since the isovaleramide analogue **10b** provided the most potent BIR2 inhibitor, it was held constant while variation in the R2 region was explored in an effort to identify a naphthyl replacement with increased BIR2 potency. The selection of substituents was guided by the R2 region SAR from the benzoxazepinone series, where aromatic groups were preferred

dx.doi.org/10.1021/jm400732v | J. Med. Chem. XXXX, XXX, XXX−XXX

Table 1. Initial SAR Exploration of *N*-Substituents

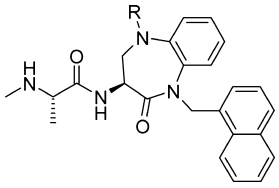

compd[a]	R	BIR2 IC_{50} (μM)[b]	BIR3 IC_{50} (μM)[b]
9	H	4.39 ± 0.45 (2)	>54.8 (2)
10a	Ac	0.928 ± 0.35 (3)	>54.8 (4)
10b	*i*-BuCO	0.611 ± 0.11 (4)	>54.8 (4)
12a	Me	4.36 ± 0.40 (2)	>54.0 (2)
12b	isopentyl	2.62 ± 0.28 (2)	>54.0 (2)

[a]All compounds were HCl salts. [b]Values are reported as mean ± SD (number of determinations).

in this position. For synthetic efficiency, the route was modified to install the R2 region substituent at the end of the synthesis (Scheme 3). Starting from benzodiazepinone **6**, deprotection and amide coupling afforded intermediate **13**, which was selectively acylated on the aniline nitrogen by treatment with isovaleryl chloride to yield **14**. The R2 region substitution was introduced via alkylation with the appropriate alkyl bromide and cesium carbonate, followed by BOC deprotection with HCl to yield compounds **15a–c**. Compounds **18** and **21a** were prepared as shown in Scheme 4, using chemistry analogous to that described for Scheme 1.

Scheme 3. Synthesis of Analogues to Explore the R2 Region[a]

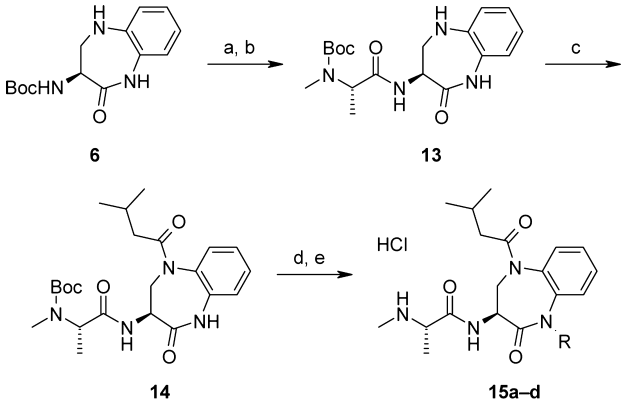

[a]Reagents and conditions: (a) HCl, 1,4-diox, rt; (b) Boc-*N*-methyl-L-alanine, HBPyU, HOBt, *i*-Pr_2NEt, DMF, 0 °C to rt, quant (2 steps); (c) *i*-BuCOCl, pyr, CH_2Cl_2, 0 °C to rt, 84%; (d) RBr, Cs_2CO_3, DMF, 100 °C; (e) HCl, 1,4-diox, rt., 32%–quant (2 steps).

In the R2 region of the molecule, it was observed that while the benzyl and phenethyl derivatives (**15a** and **15b**, respectively, Table 2) retain some BIR2 potency, they are not as potent as the naphthyl derivatives. Addition of an α-methyl group, compound **15c**, caused an approximately 4-fold loss of potency over the unsubstituted naphthyl compound **10b**, whereas the addition of a substituent at the 2-position of the naphthyl ring resulted in increased BIR2 potency. The 2-methylnaphthyl analogue **18** is about twice as potent as the unsubstituted analogue **10b**, and the 2-methoxynaphthyl ring in analogue **15d** provides another 2-fold increase over analogue **18**. It was the 6-bromo-2-methoxynaphthyl analogue **21a** that provided the most potent and first double-digit nanomolar compound, which was 10-fold more potent than the unsubstituted naphthyl **10b**. This SAR trend paralleled very closely that which was observed for the benzoxazepinone series, allowing the team to work on both series at the same time and transfer SAR lessons between the series and decrease the optimization time. Because the CYP3A4 inhibition was a known liability of the benzoxazepinone series, CYP3A4 inhibition data for all new derivatives was obtained and was used in conjunction with potency to guide the optimization of the benzodiazepinone series. While this effort in the R2 region brought the BIR2 potency into the desired range, the most potent analogues still had a CYP liability.

In an attempt to address the CYP inhibition problem, we retained the most potent 6-bromo-2-methoxynaphthyl group and revisited the R1 region with the aim of identifying substituents that would maintain the BIR2 potency and selectivity while increasing the CYP3A4 IC_{50}. The compounds were prepared as shown in Scheme 4, with methods analogous to those described for Scheme 1. We initially examined a selection of aromatic amides, ranging from the unsubstituted phenyl **21b** through a variety of substituted phenyl analogues **21c–j** (Table 3). These compounds were all very potent, with little deviation in activity against the BIR2 domain (IC_{50} 6–35 nM). Substitution on the phenyl ring did not significantly affect potency and the substituent position also had little effect, as illustrated by the *para*-, *meta*-, and *ortho*-fluoro substituted compounds **21c–e** which all have similar potency. The

Scheme 4. Synthesis of *N*-Acyl Analogues[a]

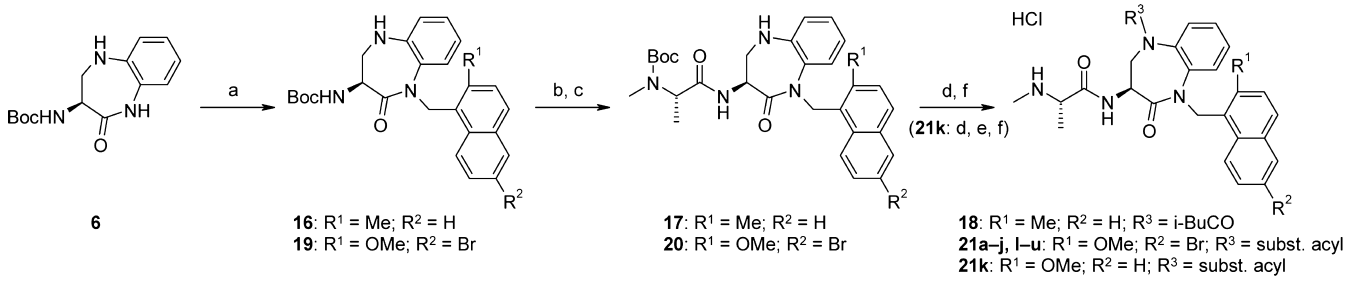

[a]Reagents and conditions: (a) LiHMDS, THF, −78 °C; for **16**, 1-(chloromethyl)-2-methylnaphthalene, KI, 69%; for **19**, 6-bromo-1-(chloromethyl)-2-methoxynaphthalene, NaI, 92%; (b) HCl, 1,4-diox, rt; (c) Boc-*N*-methyl-L-alanine, HBPyU, HOBt, *i*-Pr_2NEt, DMF, 0 °C to rt, 90%–quant (2 steps); (d) for **18**, *i*-BuCOCl, Et_3N, CH_2Cl_2, rt, 74%; for **21a–u** (except **21r**, which was made by a different route, see Supporting Information), R^3COCl, pyr, CH_2Cl_2, 60–95% or R^3CO_2H, $POCl_3$, pyr, 40%–quant; (e) for **21k**, H_2 (50 psi), 10% Pd/C, MeOH, rt; (f) HCl, 1,4-diox, rt, 69%–quant, or HCl, Et_2O, MeOH, rt, 78%–quant.

dx.doi.org/10.1021/jm400732v | J. Med. Chem. XXXX, XXX, XXX–XXX

Table 2. Initial Exploration of the Naphthyl Region

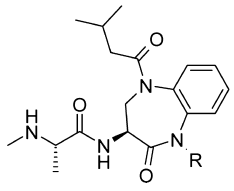

Compound[a]	R	BIR2 IC_{50} (μM)[b]	BIR3 IC_{50} (μM)[b]	CYP3A4 IC_{50} (μM)
10b	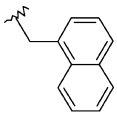	0.611 ± 0.11 (4)	>54.8 (4)	1.8
15a	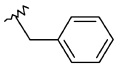	2.77 ± 0.24 (2)	>54.8 (2)	15
15b	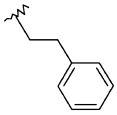	6.75 ± 0.00 (2)	>54.8 (2)	3.3
15c	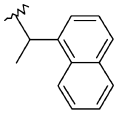	2.23 ± 0.09 (2)	>54.8 (1)	n.t.[c]
18	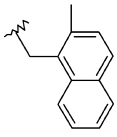	0.383 ± 0.090 (4)	>54.8 (3)	1.3
15d	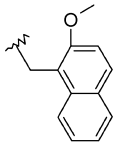	0.150	>54.8	1.5
21a	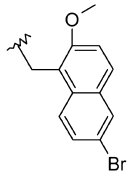	0.058 ± 0.032 (3)	>54.8 (3)	1.1

[a]All compounds were HCl salts. [b]Values are reported as mean ± SD (number of determinations). [c]Not tested, the compound was not evaluated in this assay.

electronic nature of the phenyl substituent also did not significantly impact potency. Phenyl rings with electron-withdrawing groups ranged in potency from 6 nM for the 4-(methylsulfone) substitution of **21g** to 35 nM for the 4-nitrophenyl analogue **21i**, while the electron-donating methyl group in **21f** is 6 nM. The substituted-phenyl compounds all retained high selectivity over BIR3 (>1000-fold), however, the CYP3A4 inhibition remained an issue for most compounds. Only the aniline analogue **21j**, which was formed by reduction of the nitro group of the precursor **21i** and which proceeded with concomitant hydrogenolysis of the bromine of the naphthyl moiety, had an improved CYP3A4 inhibition. This compound was not pursued further due to the potential liabilities of the aniline moiety. Heteroaromatic groups such as pyridine, pyrimidine, and furan, **21k–n**, have single-digit nanomolar potency at BIR2 but did not demonstrate any advantage regarding the CYP3A4 inhibition liability. The first evidence of being able to modulate CYP3A4 inhibition while retaining BIR2 potency came during the exploration of aliphatic amides. The acetate **21p** and the tetrahydropyranylcarboxylate **21o** were found to have good BIR2 potency with modest improvements in CYP3A4 inhibition. The greatest improvement in CYP3A4 inhibition came with the polar 2-(methylsulfonyl)acetate analogue **21q** that displayed 9 nM potency at BIR2 and a CYP3A4 IC_{50} of 10 μM. This promising result validated our hypothesis that we could use this region of the molecule to modulate the CYP3A4 inhibition in a manner unavailable to the benzoxazepinone series. In addition to the amide linker, sulfonamides, ureas, and carbamates were also evaluated, however, these analogues were not as potent (data not shown).

To better understand the binding mode and the specificity of these compounds, we obtained a crystal structure of **21j** bound to XIAP BIR2 (Figure 3).[23] Consistent with published structures of BIR2 and BIR3, the alanine sits in the P1 pocket, pointing toward the face of Trp210, with the *N*-terminus surrounded by three acidic side chains. The core amide interacts with the protein in a β-strand like fashion. The aniline and naphthyl groups branch from the benzodiazepinone core and fill the P4 area. In particular, the carbonyl of the aniline amide accepts a hydrogen bond from the side chain of Asn209, while the face of the aniline sits against Lys208, making hydrophobic interactions with its alkyl chain. In BIR3, this residue is an aspartic acid and therefore cannot donate a hydrogen bond. The 2-methoxynaphthyl group is 4 Å away from and tilted about 65° relative to the plane of the aniline and is approaching the XIAP BIR2-specific narrow hydrophobic pocket created by space between the extended side chains of Lys206 and Lys208. The naphthyl group is positioned near Phe224 which is a tyrosine in BIR3 and, presumably, the hydroxyl group of the tyrosine would have an unfavorable interaction with the naphthyl, contributing to the BIR2 specificity of these compounds. Overall, the binding mode is similar to that observed with the benzoxazepinone series and supports our use of the SAR of that series to develop the foundation of the benzodiazepinone series and set the stage for subsequent optimization.

Because sulfone **21q** was very potent and selective for BIR2 and had an acceptable CYP3A4 inhibition value, it was progressed into a PK study in C57 mice. This compound exhibited moderately high clearance (Table 4, 29 mL/min/kg), similar to the benzazepinone and benzoxazepinone series. In the benzazepinone series, metabolite identification studies showed that amide hydrolysis by an extrahepatic mechanism was one of the routes of clearance,[20] and we believed a similar mechanism could be operative in this series. In the benzoxazepinone series, an improvement in metabolic stability was observed with an increase in steric bulk adjacent to the amide bond. It was believed that the same strategy in the benzodiazepinone series might produce a more metabolically stable compound as well. To examine this hypothesis, we targeted the analogue of **21q** that has a *trans*-methyl group at the 4-position of the benzodiazepinone core. This configuration was chosen based on ease of access from intermediates derived from L-threonine.

The synthesis of the *trans*-methyl benzodiazepinone began with the nucleophilic substitution of the fluorine of 1-fluoro-2-nitrobenzene with the free amine of (2*S*,3*S*)-methyl 3-amino-2-

dx.doi.org/10.1021/jm400732v | J. Med. Chem. XXXX, XXX, XXX–XXX

Table 3. Exploration of R1 Region Amides

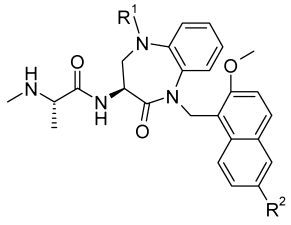

21a–i, k-q : R^2 = Br
21j: R^2 = H

Compound[a]	R^1	BIR2 IC_{50} (μM)[b]	BIR3 IC_{50} (μM)[b]	CYP3A4 IC_{50} (μM)
21a	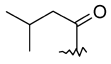	0.058 ± 0.032 (3)	>54.8 (3)	1.1
21b	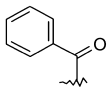	0.006	24.8	1.2
21c	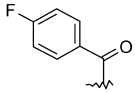	0.008	27.0	1.5
21d	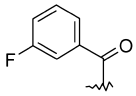	0.011	27.0	1.2
21e	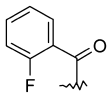	0.011	24.3	0.86
21f	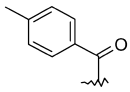	0.006	30.3	1.4
21g	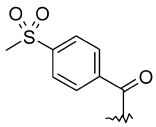	0.006	25.7	2.0
21h	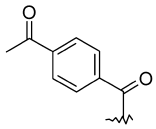	0.022 ± 0.015 (8)	39.3 ± 13.8 (7)	1.8
21i	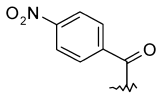	0.035 ± 0.003 (2)	>54.8	n.t.[c]
21j	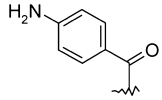	0.006 ± 0.002 (5)	24.5 ± 6.1 (7)	10.2
21k	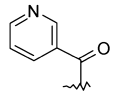	0.005	17.0	1.2
21l	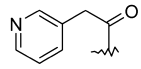	0.007	42.7	2.8
21m	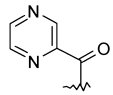	0.009	45.9	1.6
21n	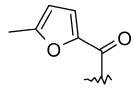	0.006	30.6	1.9
21o	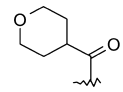	0.006	18.2	2.3
21p		0.015	>54.8	3.2
21q	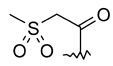	0.009	>54.8	10.0

[a]All compounds were HCl salts. [b]Values that are the result of multiple determinations are reported as mean ± SD (number of determinations). [c]Not tested, the compound was not evaluated in this assay.

(*tert*-butoxycarbonylamino)butanoate (**22**),[24] followed by saponification of the methyl ester, reduction of the nitro group by catalytic hydrogenation, and then cyclization under amide coupling conditions to provide the benzodiazepinone core **23** (Scheme 5). Under conditions similar to those described above, the nitrogen was acylated using the acid chloride generated in situ from 2-(methanesulfonyl)acetic acid to provide **24** and the *N*-methyl-L-alanine chain was installed, giving **25**. In the final set of steps, the R2 moiety was installed via alkylation of **25** with 6-bromo-1-(chloromethyl)-2-methoxynaphthalene in the presence of sodium iodide and cesium carbonate, and then acidic deprotection of the amine yielded compound **26a**.

The modifications resulting in **26a** did, indeed, reduce the clearance in mouse from 28.9 mL/min/kg for **21q** to 7.5 mL/min/kg for **26a**, but the CYP3A4 IC_{50} of 4.8 μM was now a concern (Table 5). We profiled **26a** for CYP3A4 TDI and found this compound was a potent time-dependent inhibitor. The CYP3A4 TDI assay used was a modification of that described by Chen and co-workers[25] in which k_{obs} values for loss of enzyme activity in human liver microsomes over 30 min were determined in the presence of 10 and 50 μM concentrations of test compound. The TDI kinetic parameters K_I and k_{inact} were then estimated using Kitz–Wilson plots, and the inactivation potency is represented by the ratio k_{inact}/K_I. In the case of compound **26a**, the k_{obs} values indicated that it was a highly potent time-dependent inhibitor at both concentrations tested, but characteristics of the curves prevented the estimation of K_I and k_{inact}.

dx.doi.org/10.1021/jm400732v | J. Med. Chem. XXXX, XXX, XXX–XXX

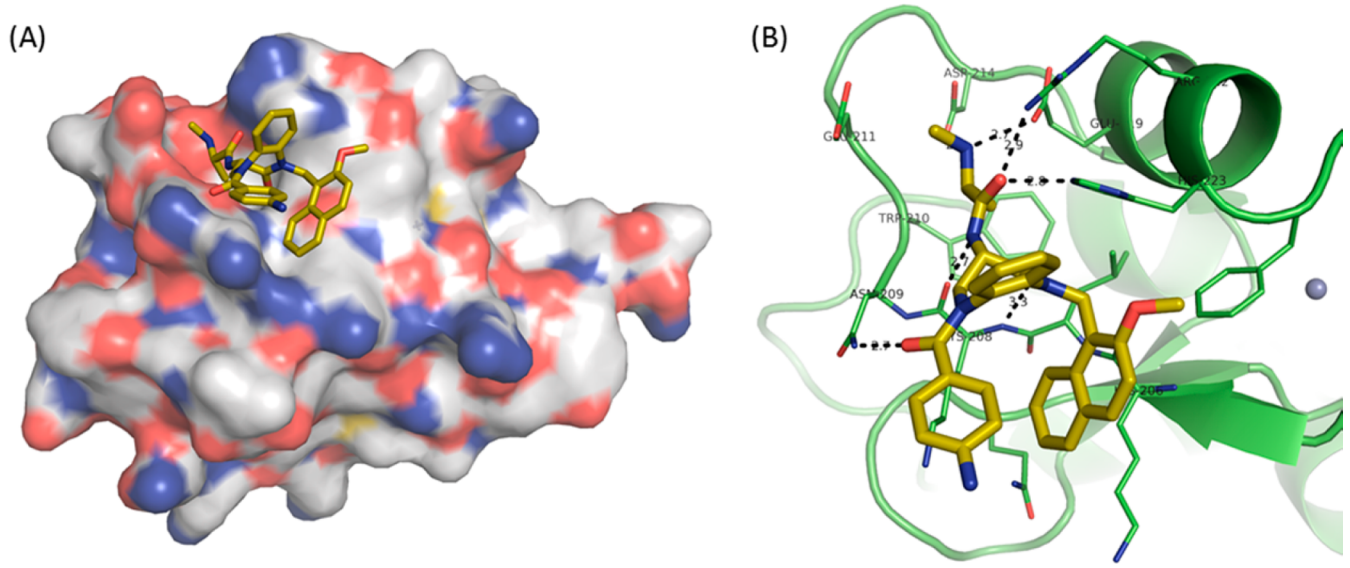

Figure 3. X-ray cocrystal structure of **21j** with XIAP BIR2 domain. (A) The protein is represented as an electrostatic surface. (B) Interactions of the ligand with the peptide-binding groove of the protein. H-bonding interactions between the protein and ligand are represented by black dotted lines labeled with the distance.

Table 4. PK Properties of 21q

property	value for **21q**[a]
CL (mL/min/kg)	28.9
V_{ss} (L/kg)	1.14
AUC (ng·h/mL)	285

[a]Mouse cassette iv PK study, compound dosed iv at 0.5 mg/kg.

Retaining the *trans*-methyl group on the diazepinone core and the sulfone moiety in R1, attention was directed at identifying modifications to the naphthyl region (R2) that would lead to improvements in the TDI and CYP3A4 inhibition issues. The synthesis of compounds **26b–g** was carried out according to the protocols described in Scheme 5, and they were profiled in the CYP3A4 inhibition and TDI assays and in cassette PK in C57 mice (Table 6). Moving the bromine to the 5-position in **26b** served to decrease the CYP3A4 IC_{50} by almost 3-fold (1.7 μM) and had little effect on the other properties. The bromine group was removed in **26c**, which retained similar potency at BIR2, increased the CYP3A4

Scheme 5. Preparation of *trans*-Methyl Benzodiazepinone Analogues[a]

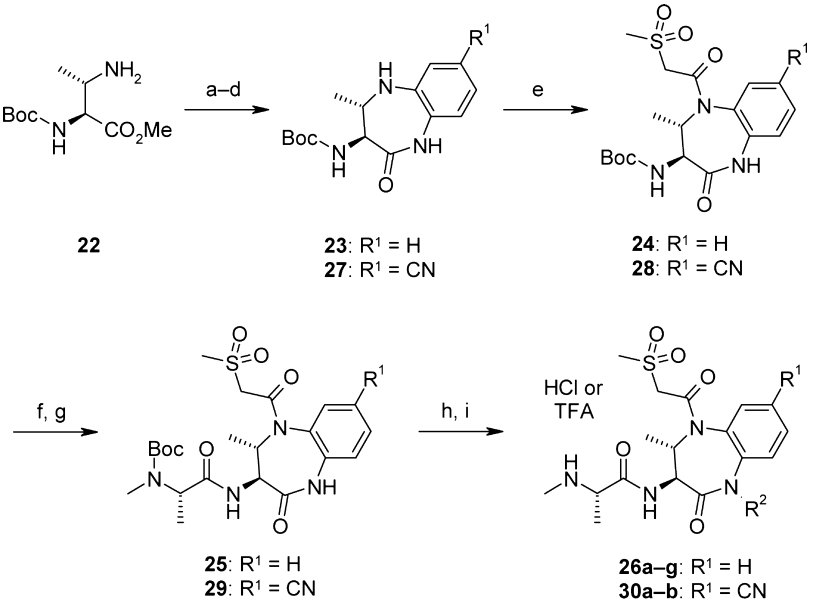

[a]Reagents and conditions: To prepare **26a**, the order of steps from **24** was: h, f, g, i. (a) 1-Fluoro-2-nitrobenzene for **23** or 3-fluoro-4-nitrobenzonitrile for **27**, $NaHCO_3$, DMF, 85 °C, 78%; (b) LiOH, H_2O–1,4-diox, rt; (c) H_2, Pd/C, EtOH, rt; (d) EDCI, DMF, rt, 91% (3 steps) for **23**, 16% (3 steps) for **27**; (e) methanesulfonylacetic acid, $POCl_3$, pyr, 0 °C, 89–94%; (f) for **25**, TFA, CH_2Cl_2, rt; for **29**, HCl, 1,4-diox, rt; (g) Boc-*N*-methyl-L-alanine, HBTU, *i*-Pr_2NEt, DMF, 0 °C to rt, 74–91% (2 steps); (h) R^2 bromide or chloride, Cs_2CO_3, NaI, DMF, rt, 38–90%; (i) HCl, 1,4-diox, rt or Et_2O–MeOH, rt or TFA, CH_2Cl_2, rt.

dx.doi.org/10.1021/jm400732v | J. Med. Chem. XXXX, XXX, XXX–XXX

Table 5. XIAP Activity, CYP3A4 Properties, and PK Properties of 26a

property	26a
XIAP activity	
BIR2 IC_{50} (μM)[a]	0.010
BIR3 IC_{50} (μM)[a]	29.2
CYP3A4	
CYP3A4 IC_{50} (μM)	4.8
CYP3A4 TDI	potent[b]
Mouse iv PK[c]	
CL (mL/min/kg)	7.5
V_{ss} (L/kg)	1.1
AUC (ng·h/mL)	2220
C_{max} (ng/mL)	1310

[a]Values are the result of a single determination. [b]k_{obs} values indicated potent TDI, but K_I and k_{inact} values could not be estimated due to characteristics of the curves. [c]Mouse cassette PK study, compound dosed iv at 1 mg/kg.

IC_{50} by about 2-fold, and improved the TDI compared with **26a**. However the clearance in mouse increased to 14 mL/min/kg, twice that of **26a**. While the 2-methylnaphthyl compound **26d** had lower potency at BIR2, as expected, it possessed the highest CYP3A4 IC_{50} value observed so far (32 μM). This compound also displayed a modest improvement in TDI, although the k_{inact}/K_I ratio was still unacceptable. These improvements came at the price of clearance, as compound **26d** had a clearance three times that of **26a**. Replacement of the naphthyl group with more polar heterocycles including benzoisoxazole, **26e**, *N*-methyl indazole, **26f**, and *N*-2-(cyanophenyl)-indazole, **26g**, resulted in compounds with BIR2 potencies ranging from 182 to 32 nM. Molecular modeling suggested the cyano group in the naphthyl replacement for **26g** would displace a water molecule in the crystal structure and make a hydrogen bond to the protein. While the replacement of the naphthyl group with these heterocycles led to improvements in the CYP 3A4 inhibition and favorable TDI for **26g**, clearance values in mouse were variable and, in the case of compound **26f**, was greater than mouse liver blood flow. While this approach did not provide a single molecule in which all the issues were addressed successfully, it did indicate that the 2-methoxynaphthyl and 2-methylnaphthyl groups provided a favorable balance of properties and could serve as acceptable R2 groups if the CYP inhibition and TDI issues could be further improved by modifications elsewhere.

At this point, the only area of the molecule that had not been modified was the phenyl ring of the benzodiazepinone system. We hypothesized that the phenyl ring of the core could potentially be oxidized to a reactive intermediate/metabolite that could account for the high TDI observed with these compounds. By making the ring more electron deficient, we might be able to mitigate this. Preliminary investigations indicated that cyano-substitution at the 7-position of the benzodiazepinone was tolerated, so we combined that with the two best R2 region groups, 2-methoxynaphthyl and 2-methylnapthyl, to give compounds **30a** and **30b** (the synthesis was carried out according to the protocols described in Scheme 5). These analogues exhibited a 2-fold improvement in potency at the BIR2 domain over the unsubstituted compounds **26c** and **26d** (Table 7). The in vitro safety data on these two compounds also showed a considerable improvement. The electron withdrawing groups added to the phenyl ring produced compounds with a low TDI signal and they also possessed a higher IC_{50} for CYP3A4. These were the first compounds that satisfied our potency, selectivity, and in vitro safety criteria. However, the clearance for **30a** was approximately 3-fold greater than the unsubstituted compound **26c**, and for compound **30b** the clearance was approximately the same as the unsubstituted compound **26d**. In both cases, we believed the clearance could be improved.

In the final attempt at identifying a compound with all the desired attributes, a decision was made to re-explore the R1 amide region. The initial group selected for chemistry optimization work was the acetyl group. The synthetic scheme to prepare these analogues was not as flexible as that for the earlier analogues. Attempts to acetylate **27** proceeded without selectivity for the aniline nitrogen and led to a mixture of mono- and bis-acylated products. This was addressed by installing the naphthyl group first (Scheme 6). Alkylation of the benzodiazepinone core **27** with the appropriately substituted chloromethylnaphthalene provided **31** and **34**. These were then acylated with acetyl chloride to provide **32** and **35**. The *N*-methyl-L-alanine moiety was installed according to the standard procedure, providing the final compounds **33** and **36**.

Compounds **33** and **36** represented an optimal combination of substitutions that when tested in our assays possessed the key attributes of low TDI, low metabolic clearance in vivo, and a lowered potential for CYP3A4 inhibition (data summarized in Table 8). These two compounds were roughly equipotent at the BIR2 domain of XIAP and retained excellent selectivity against the BIR3 domain. They were also devoid of any in vitro safety flags. Replacing the 2-(methylsulfonyl)-acetyl group with the acetyl group caused a slight decrease in the CYP3A4 inhibition value, but it was still in an acceptable range and the TDI was low. Additionally, these compounds showed no significant inhibition of the CYP2D6 and CYP2C9 isoforms. Because benzoxazepinone **4** promoted CYP3A4 induction, we tested for this with **36** and did not observe any induction at concentrations of **36** up to 10 μM. In further profiling, no GSH adducts were observed in a GSH trapping assay for either **33** or **36**, and hERG inhibition was acceptable. Comparing these analogues to the 2-(methylsulfonyl)-acetyl compounds **30a** and **30b**, the greatest improvement was in their PK properties. The clearance values for **33** and **36** were the lowest observed in this series. Compound **33** exhibited modest oral bioavailability, while **36** had 28% bioavailability. We decided to progress compound **36** as our lead molecule based primarily on differences in protein binding. For **36**, the free fraction in mouse and human was comparable (0.51% vs 1.6%), whereas compound **33** showed a nearly 35-fold difference (0.08% vs 2.79%), which might result in issues in further development.

Compound **36** was also tested for activity against the BIR2 and BIR3 domains of cIAP1 and was found to have high selectivity for XIAP, with 58-fold selectivity against cIAP1 BIR2 (Table 9). Compound **36** was then evaluated in a caspase reactivation functional assay designed to support the proposed mechanism of action. Endogenous caspases obtained from HeLa S3 cell lysates were activated by treatment with cytochrome c and ATP and inhibited by the addition of full-length XIAP. The subsequent addition of **36** restored caspase activity in a dose-dependent manner with an EC_{50} of 0.262 μM, measured by the cleavage of Ac-DEVD-AFC, a fluorogenic substrate specific for caspases 3 and 7. This confirms the

dx.doi.org/10.1021/jm400732v | J. Med. Chem. XXXX, XXX, XXX−XXX

Table 6. Exploration of the R2 region of *trans*-Methyl Benzodiazepinone Core

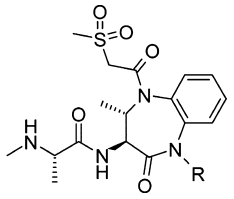

Compound[a]	R	BIR2 IC_{50} (μM)[b]	BIR3 IC_{50} (μM)[b]	CYP3A4 IC_{50} (μM)	CYP3A4 TDI K_I (μM)	CYP3A4 TDI k_{inact} (min^{-1})	CYP3A4 TDI k_{inact}/K_I	CL (mL/min/kg)[c]
26a	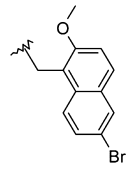	0.010	29.2	4.8	Potent[d]	Potent[d]	Potent[d]	7.5
26b	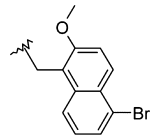	0.009	24.9	1.7	n.d.[e]	n.d.[e]	n.d.[e]	7.1
26c	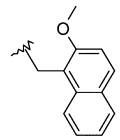	0.019 ± 0.000 (2)	>54.8 (2)	9.7	7.1	0.021	0.0030	14
26d	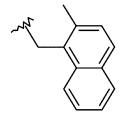	0.058	>54.8	32	8.5	0.022	0.0026	24
26e	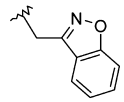	0.182	>54.8	38	2.1	0.009	0.0041	59
26f	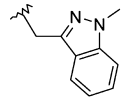	0.083	>54.8	>50	n.t.[f]	n.t.[f]	n.t.[f]	149
26g	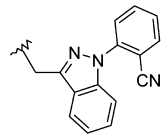	0.032	>54.8	37	83.3	0.019	0.0002	31

[a]Compounds were HCl salts, except **26e** which was a TFA salt. [b]Values that are the result of multiple determinations are reported as mean ± SD (number of determinations). [c]Mouse cassette PK study, compound dosed iv at 0.5 mg/kg except **26a–c**, which were dosed at 1 mg/kg. [d]k_{obs} values indicated potent TDI, but K_I and k_{inact} values could not be estimated due to characteristics of the curves. [e]Not determined, unable to estimate K_I and k_{inact} due to potent reversible inhibition. [f]Not tested, the compound was not evaluated in this assay.

relationship between XIAP BIR2 inhibition and apoptotic signaling in accordance with the mechanistic proposal.

To determine whether **36** maintained its activity in cellular systems, it was evaluated in a 5 day cell viability assay using SW620 cells. While compound **36** showed no single agent activity in the cellular assay, it had a significant effect on cell viability when dosed in combination with the DR5 antibody, conatumumab, which serves to activate the apoptotic signaling through the extrinsic pathway, and dose–response curves for the DR5 antibody alone and in the presence of increasing concentrations of **36** (0.37, 1.1, 3.3, and 10 μM) (Figure 4A) were generated. In the absence of test compound, no significant growth inhibition was observed. The combination of DR5 antibody and compound **36** exhibited a dose-dependent increase in cell growth inhibition, indicating that **36** is effective at sensitizing the SW620 cells to conatumumab. Similar growth inhibition behavior was observed with the BIR3-selective compound **3** (Figure 4B). Compounds **3** and **36** were also tested in other cell lines and showed similar activity (see Supporting Information, Figure 1). The selectivity of compound **36** for XIAP over cIAP was expected to decrease or eliminate the TNFα secretion observed with BIR3 antagonists, such as **3**. To confirm this, TNFα levels were measured following the treatment of MDA-MB-231[26] cells with either **36** or **3** (Figure 4C). No significant TNFα induction was observed with the BIR2-selective compound **36**, while **3**

dx.doi.org/10.1021/jm400732v | J. Med. Chem. XXXX, XXX, XXX–XXX

Table 7. Cyano-Substituted Compounds

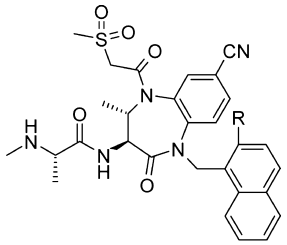

compd[a]	R	BIR2 IC_{50} (μM)[b]	BIR3 IC_{50} (μM)[b]	CYP3A4 IC_{50} (μM)	CYP3A4 TDI K_I (μM)	CYP3A4 TDI k_{inact} (min^{-1})	CYP3A4 TDI k_{inact}/K_I	CL (mL/min/kg)[c]
30a	OMe	0.010	12.9	>50	50	0.006	0.001	46.4
30b	Me	0.051 ± 0.003 (2)	37.8 ± 0.2 (2)	>50	50	0.012	0.002	21.3

[a]All compounds were HCl salts. [b]Values that are the result of multiple determinations are reported as: Mean ± SD (number of determinations). [c]Mouse cassette PK study, compound dosed iv at 0.5 mg/kg.

Scheme 6. Synthesis of Optimized Benzodiazepinone Analogues[a]

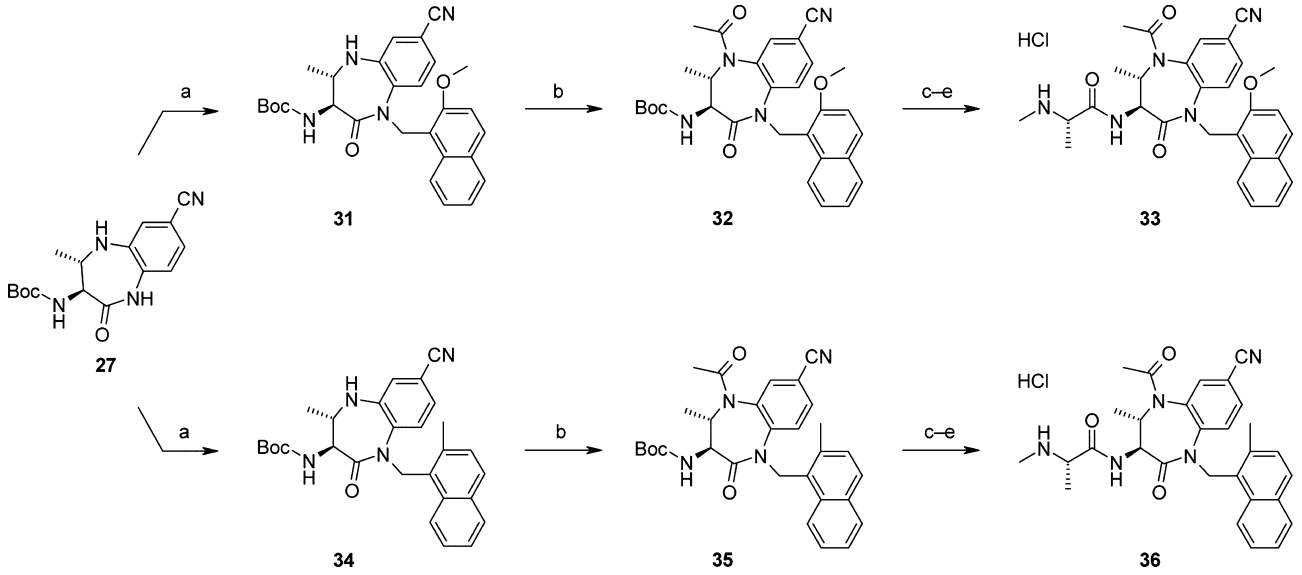

[a]Reagents and conditions: (a) 1-(chloromethyl)-2-methoxynaphthalene or 1-(chloromethyl)-2-methoxynaphthalene, Cs_2CO_3, NaI, DMF, rt, 72–80%; (b) AcCl, pyr, CH_2Cl_2, 0 °C, 59–65%; (c) HCl, 1,4-diox, rt; (d) Boc-*N*-methyl-L-alanine, HBTU, *i*-Pr_2NEt, DMF, 0 °C to rt, 69–70%; (e) HCl, 1,4-diox, rt, 80–87%.

showed high TNFα levels at all concentrations where cellular activity was observed. The production of TNFα by BIR3-selective compounds is thought to arise from cIAP degradation, promoted by compound binding, which serves to activate the noncanonical NF-κB pathway.[18] Compound **21j**, a closely related analogue of **36**, did not promote degradation of cIAP1 in CHL-1 cells, where the BIR3-selective compound **3** did (see Supporting Information, Figure 2).

The compounds were then evaluated in a pharmacodynamic model designed to measure the level of caspase 3 and 7 activity. Compound **36**, XIAP BIR2 selective antagonist, and compound **3**, pan-IAP BIR3 antagonist, were examined in combination with conatumumab in nude mice implanted with LOX melanoma xenografts (Figure 4D). The compounds were administered as single doses (1 mg/kg ip for conatumumab, 200 mg/kg po for **36**, and 100 mg/kg po for **3**), and the xenografts were removed after 8 h and analyzed for caspase 3 and 7 activity. The LOX cell line is sensitive to the DR5 antibody, resulting in elevated caspase 3 and 7 levels upon treatment with conatumumab alone. While compound treatment alone resulted in little caspase 3 and 7 activity, in combination they significantly potentiated the activity of conatumumab and **36** displayed a level of activity comparable to that of **3**.

CONCLUSION

While pan-IAP inhibitors with selectivity for the BIR3 domain of XIAP, cIAP1, and cIAP2 have been reported in the literature, this, with our previous papers,[20,21] is the first disclosure of a highly potent and selective XIAP BIR2 inhibitor. The discovery of benzodiazepinone **36** was driven by the iterative optimization of safety properties, CYP3A4 inhibition and TDI, starting from compound **9**. During the course of this optimization, poor clearance in vivo was an issue and was addressed by the placement of a *trans*-methyl group onto the core diazepinone ring, resulting in a compound suitable for in vivo studies. Compound **36** is highly potent and selective for XIAP BIR2 (~700-fold selective over XIAP BIR3 and 58-fold

dx.doi.org/10.1021/jm400732v | J. Med. Chem. XXXX, XXX, XXX–XXX

Table 8. XIAP, in Vitro Safety, and PK Properties of 33 and 36

property	33	36
XIAP Activity		
XIAP BIR2 IC_{50} (μM)[a]	0.022 ± 0.008 (2)	0.045 ± 0.006 (3)
XIAP BIR3 IC_{50} (μM)[a]	23.2 ± 8.5 (2)	30.8 ± 3.18 (3)
in Vitro Safety		
CYP3A4 IC_{50} (μM)	18	16
CYP2D6 IC_{50} (μM)	>50	>50
CYP2C9 IC_{50} (μM)	>50	>50
CYP3A4 TDI K_I (μM)	50	16.7
CYP3A4 TDI k_{inact} (min^{-1})	0.018	0.008
CYP3A4 TDI k_{inact}/K_I (L/min/μmol)	0.0004	0.0005
CYP 3A4 induction	n.t.[b]	no flag[c]
GSH adduct formation	no flag	no flag
hERG IC_{20} (μM)	>10	8.84
hERG IC_{50} (μM)	>20	35.3
mouse iv PK[d]		
CL (mL/min/kg)	3.0	4.3
V_{ss} (L/kg)	0.52	0.98
AUC (ng·h/mL)	3032	1378
C_{max} (ng/mL)	1555	792
mouse po PK[e]		
AUC (ng·h/mL)	5980	7870
C_{max} (ng/mL)	873	823
T_{max} (h)	4.0	0.25
F (%)	8	28
Protein Binding		
mouse (% free)	0.08	0.51
human (% free)	2.8	1.6

[a]Values are reported as: Mean ± SD (number of determinations). [b]Not tested, compound was not evaluated in this assay. [c]No significant increase in CYP3A4 mRNA compared to control at up to 10 μM **36**. [d]Mouse cassette PK study, compound dosed iv at 0.5 mg/kg. [e]Mouse single-dose PK study, compound dosed po at 10 mg/kg.

Table 9. Biological Characterization of 36

property	value[a]
XIAP Activity	
BIR2 IC_{50} (μM)	0.045 ± 0.006 (3)
BIR3 IC_{50} (μM)	30.8 ± 3.2 (3)
cIAP1 Activity	
BIR2 IC_{50} (μM)	2.64
BIR3 IC_{50} (μM)	>54.8
XIAP-Caspase Reactivation	
EC_{50} (μM)	0.262 ± 0.024 (2)

[a]Values that are the result of multiple determinations are reported as mean ± SD (number of determinations).

selective over cIAP1 BIR2) and has acceptable safety and PK properties. This represents a substantial improvement in selectivity compared to the benzoxazepinone analogue reported in our previous paper, which was used to establish proof of concept for this mechanism. In combination with the DR5 antibody conatumumab, **36** demonstrated cellular efficacy and increased caspase 3 and 7 activity in a PD study in mouse xenografts. This activity does not proceed through pathways involving cIAP inhibition and TNFα release, differentiating **36** from known BIR3 inhibitors. Compound **36** will be profiled further in a tumor growth inhibition xenograft study and toxicology studies.

EXPERIMENTAL SECTION

Chemistry. *General.* Experimental procedures are given below for the preparation of **30a−b**, **33**, and **36** (including intermediates **27−35**). All commercially available reactants, reagents, and solvents were used as received. Reactions using air- or moisture-sensitive reagents were performed under an atmosphere of Ar or N_2. Reactions were monitored by LC-MS or TLC. Flash chromatography was performed with Isco CombiFlash Companion or AnaLogix IntelliFlash chromatography systems using prepacked silica gel columns (40−60 μm particle size RediSep or 20−40 μm spherical silica gel RediSep Gold columns purchased from Teledyne Isco, or comparable products from other vendors). Preparative HPLC was performed using a Waters HPLC system consisting of a 2767 sample manager, 2525 binary gradient module, and 2996 photodiode array detector with a SunFire Prep C18 OBD column (5 μm, 30 mm × 100 mm) eluted with a 10−100% MeCN−H_2O linear gradient with 0.1% v/v TFA at a flow rate of 30 mL/min, or using similar methods on a comparable system. NMR spectra were measured on Bruker 300 or 400 MHz spectrometers. Chemical shifts are reported in ppm downfield from TMS using residual nondeuterated solvent as an internal standard ($CHCl_3$, 7.26 ppm; DMSO, 2.50 ppm). Data are reported in the form: chemical shift (multiplicity, coupling constants, integration). Multiplicities are recorded by the following abbreviations: s, singlet; d, doublet; t, triplet; q, quartet; m, multiplet; br, broad. HRMS data were recorded on a ThermoFisher OrbiTrap FTMS system using flow injection with electrospray ionization in positive mode. Analytical HPLC and LC-MS analyses were performed using either Waters or Agilent LC-MS systems. The Waters system was comprised of a ZQ mass spectrometer using multimode (ES/APCI) ionization with alternating ± switching and an ES Industries Chromegabond WR C18 column (3 μm, 120 Å, 30 mm × 3.2 mm) eluted with a 10−90% MeCN−H_2O linear gradient with 0.1% v/v TFA. The Agilent system was comprised of a 6140 mass spectrometer using multimode (ES/APCI) ionization with alternating ± switching and an Agilent Zorbax SB C-18 column (3.5 μm, 30 mm × 2.1 mm) eluted with a 10−90% MeCN−H_2O linear gradient with 0.1% v/v TFA. All tested compounds were evaluated on one of these analytical HPLC systems and determined to be ≥95% pure.

*tert-Butyl (3S,4S)-7-Cyano-4-methyl-2-oxo-2,3,4,5-tetrahydro-1H-benzo[b][1,4]diazepin-3-ylcarbamate (**27**). Step 1.* A suspension of **22** (6.49 g, 27.9 mmol), 3-fluoro-4-nitrobenzonitrile (6.96 g, 41.9 mmol), and sodium bicarbonate (7.04 g, 83.8 mmol) in DMF was stirred at 65 °C for 3 h. The reaction was cooled and concentrated. The residue was diluted with H_2O (100 mL) and extracted with EtOAc (2 × 150 mL). The combined organic layers were washed with H_2O (50 mL) and satd aq NaCl (50 mL), dried over Na_2SO_4, filtered, and concentrated. The crude material was purified by flash chromatography (330 g silica gel; 5−50% EtOAc−hexanes) to provide (2*S*,3*S*)-methyl 2-(*tert*-butoxycarbonylamino)-3-(5-cyano-2-nitrophenylamino)butanoate (8.2 g, 78%). ^{1}H NMR (400 MHz, DMSO-d_6) δ 8.20 (d, J = 8.8 Hz, 1H), 8.06 (d, J = 9.0 Hz, 1H), 7.66 (s, 1H), 7.59 (d, J = 8.5 Hz, 1H), 7.08 (d, J = 8.8 Hz, 1H), 4.46 (dd, J = 8.4, 4.6 Hz, 1H), 4.42−4.32 (m, 1H), 3.67 (s, 3H), 1.35 (s, 9H), 1.20 (d, J = 7.3 Hz, 3H). MS m/z 401 $[M + Na]^+$.

Step 2. To a rt solution of (2*S*,3*S*)-methyl 2-(*tert*-butoxycarbonylamino)-3-(5-cyano-2-nitrophenylamino)butanoate (8.2 g, 21.7 mmol) in 1,4-dioxane−H_2O (1:1, 80 mL) was added 1.3 M aq LiOH (41.7 mL, 54.2 mmol). The reaction was stirred for 2 h. The reaction was acidified with 0.5 M aq HCl (to pH 5) and extracted with EtOAc (2 × 100 mL). The combined organic layers were washed with H_2O (50 mL) and satd aq NaCl (50 mL), dried over Na_2SO_4, filtered, and concentrated to provide (2*S*,3*S*)-2-(*tert*-butoxycarbonylamino)-3-(5-cyano-2-nitrophenylamino)butanoic acid (7.9 g, 100%) that was used without further purification. MS m/z 365 $[M + H]^+$.

Step 3. To a rt solution of (2*S*,3*S*)-2-(*tert*-butoxycarbonylamino)-3-(5-cyano-2-nitrophenylamino)butanoic acid (7.9 g, 21.7 mmol) in MeOH (75 mL) was added 10% palladium on carbon (800 mg). The atmosphere was exchanged for H_2, and the reaction was stirred for 4 h. The mixture was filtered through Celite and concentrated to provide

dx.doi.org/10.1021/jm400732v | J. Med. Chem. XXXX, XXX, XXX−XXX

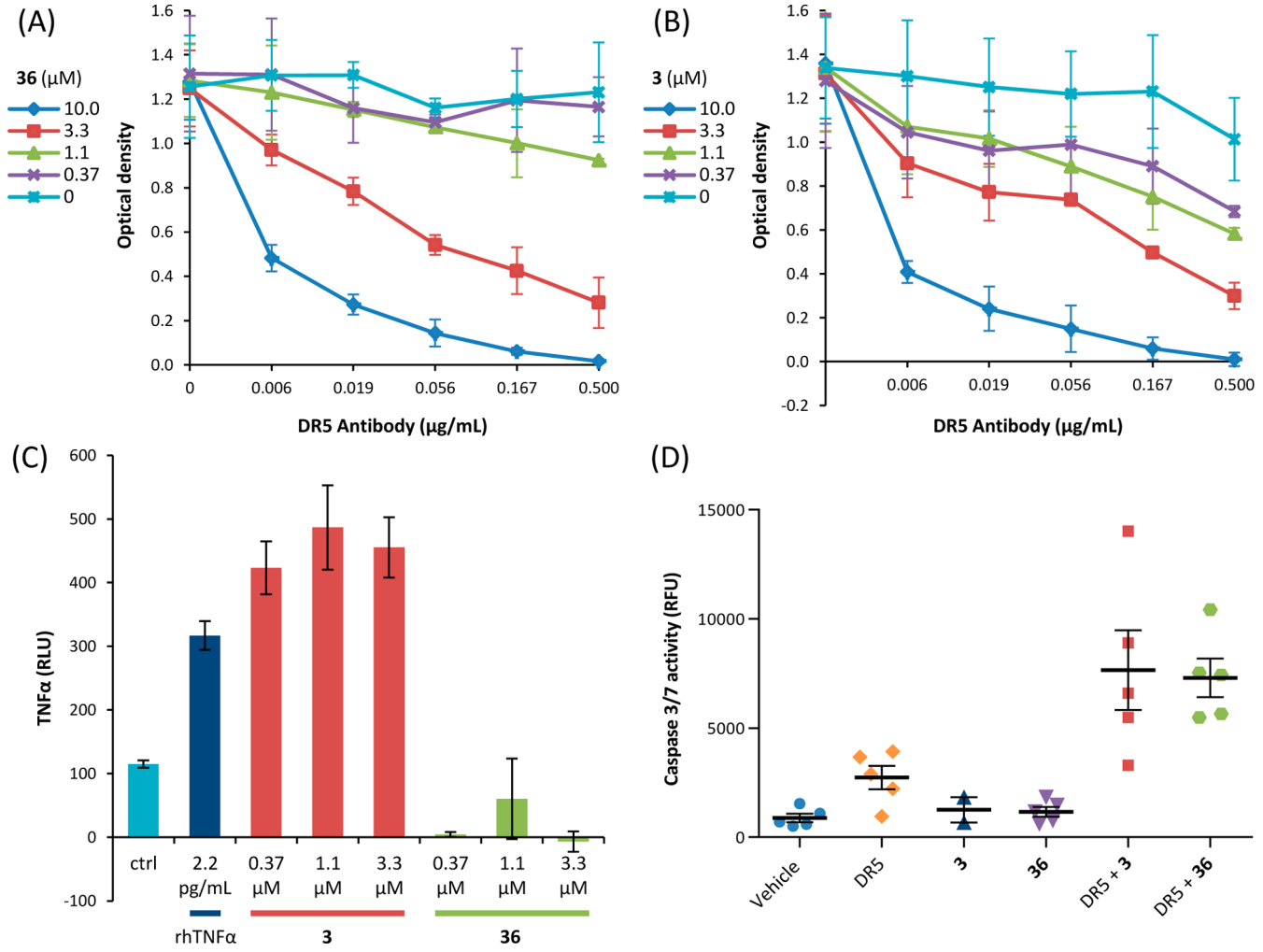

Figure 4. (A,B) Cell-based activity of **36** and **3** in combination with DR5 antibody. Proliferation of SW620 cells was evaluated in a 5 day MTS assay upon treatment with DR5 antibody in the presence of varied concentrations of **36** and **3**. At 0.5 μg/mL DR5 mAb, **36** EC_{90} = 5.23 ± 1.32 μM, **3** EC_{90} = 6.66 ± 1.51 μM. Values are the mean of two determinations ± SD. (C) Presence of TNFα in supernate from MDA-231 cells 19 h after treatment with the BIR3-selective compound **3** and BIR2-selective compound **36**. Values are the mean of two determinations ± SD. (D) The in vivo activity of **3** and **36** in combination with the DR5 mAb conatumumab in a LOX melanoma xenograft study measuring caspase 3/7 activity. Mice with LOX xenografts were dosed with conatumumab (single dose 1 mg/kg ip) and test compound (single dose 200 mg/kg po for **36**; single dose 100 mg/kg po for **3**). Xenografts were removed after 8 h, homogenized, and analyzed for caspase 3/7 enzyme activity. Mean ± SEM is indicated for each group. Concentration of the test compound in plasma and tumor at 8 h was also determined (**36**, 5.0 μM plasma, 7.7 μM tumor; **3**, 3.3 μM plasma, 18.4 μM tumor).

(2*S*,3*S*)-3-(2-amino-5-cyanophenylamino)-2-(*tert*-butoxycarbonylamino)butanoic acid (7.25 g, 100%) that was used without further purification. MS *m*/*z* 335 $[M + H]^+$.

Step 4. To a rt solution of (2*S*,3*S*)-3-(2-amino-5-cyanophenylamino)-2-(*tert*-butoxycarbonylamino)butanoic acid (7.25 g, 21.7 mmol) in DMF (85 mL) was added 1-ethyl-3-(3-dimethylaminopropyl)-carbodiimide hydrochloride (5.4 g, 28.2 mmol). The reaction was stirred overnight. The reaction was concentrated, diluted with H_2O (150 mL), and extracted with EtOAc (2 × 150 mL). The combined organic layers were washed with H_2O (50 mL), satd aq $NaHCO_3$ (50 mL), H_2O (50 mL), and satd aq NaCl, dried over Na_2SO_4, filtered, and concentrated. The crude material was purified by flash chromatography (silica gel; 20%−70% EtOAc−hexanes) to provide **27** (1.12 g, 16%). ^{1}H NMR (400 MHz, DMSO-d_6) δ 10.07 (s, 1H), 7.36−7.28 (m, 2H), 7.15 (d, *J* = 8.5 Hz, 1H), 7.10−7.03 (m, 1H), 5.41 (s, 1H), 3.77−3.60 (m, 2H), 1.36 (s, 9H), 1.12 (d, *J* = 5.8 Hz, 3H). MS *m*/*z* 317 $[M + H]^+$.

*tert-Butyl (2S,3S)-8-Cyano-2-methyl-1-(2-(methylsulfonyl)acetyl)-4-oxo-2,3,4,5-tetrahydro-1H-benzo[b][1,4]diazepin-3-ylcarbamate (**28**).* To a 0 °C solution of **27** (106 mg, 335 μmol) in pyridine (3.35 mL) was added 2-(methylsulfonyl)acetic acid (50.9 mg, 369 μmol) followed by phosphorus oxychloride (61.3 μL, 670 μmol) dropwise. The reaction was stirred at 0 °C for 30 min, then quenched by the addition of H_2O and extracted with EtOAc. The combined organic layers were washed with 1 N aq citric acid, H_2O, satd aq $NaHCO_3$, and satd aq NaCl, dried over Na_2SO_4, filtered, and concentrated. The crude material was purified by flash chromatography (12 g silica gel; 0−100% EtOAc−hexanes) to provide **28** (137 mg, 94%) as a white solid. ^{1}H NMR (300 MHz, DMSO-d_6) δ 10.44 (br s, 1H), 7.98 (d, *J* = 8.3 Hz, 1H), 7.91 (s, 1H), 7.48 (d, *J* = 9.1 Hz, 1H), 7.35 (d, *J* = 8.3 Hz, 1H), 5.07−4.91 (m, 1H), 4.14 (d, *J* = 15.5 Hz, 1H), 3.76 (dd, *J* = 11.7, 9.1 Hz, 1H), 3.66 (d, *J* = 15.5 Hz, 1H), 3.10 (s, 3H), 1.35 (s, 9H), 1.12 (d, *J* = 6.0 Hz, 3H). MS *m*/*z* 459 $[M + Na]^+$.

*tert-Butyl (S)-1-((2S,3S)-8-Cyano-2-methyl-1-(2-(methylsulfonyl)-acetyl)-4-oxo-2,3,4,5-tetrahydro-1H-benzo[b][1,4]diazepin-3-ylamino)-1-oxopropan-2-yl(methyl)carbamate (**29**). Step 1.* A rt solution of **28** (137 mg, 314 μmol) in 4 M HCl in 1,4-dioxane (1.57 mL) was stirred for 2 h. The reaction was concentrated and used without further purification. ^{1}H NMR (300 MHz, DMSO-d_6) d = 11.00 (s, 1H), 8.54 (br s, 3H), 8.09−7.94 (m, 2H), 7.38 (d, *J* = 7.9 Hz, 1H), 5.26−5.11 (m, 1H), 4.20 (d, *J* = 15.1 Hz, 1H), 3.96 (d, *J* = 10.6 Hz, 1H), 3.71 (d, *J* = 15.5 Hz, 1H), 3.09 (s, 3H), 1.28 (d, *J* = 6.4 Hz, 3H).

dx.doi.org/10.1021/jm400732v | *J. Med. Chem.* XXXX, XXX, XXX−XXX

Step 2. This material was taken up in DMF (1.05 mL), and Boc-*N*-methyl-L-alanine (70.2 mg, 345 μmol), *N*,*N*-diisopropylethylamine (217 μL, 1.26 mmol), and HBTU (131 mg, 345 μmol) were added at 0 °C. The reaction was stirred at rt for 30 min, then diluted with EtOAc, washed with H_2O, satd aq $NaHCO_3$, and satd aq NaCl, dried over Na_2SO_4, filtered, and concentrated. The crude material was purified by flash chromatography (12 g RediSep Gold silica gel; 20−100% EtOAc−hexanes) to provide **29** (121.8 mg, 74%, 2 steps) as a white solid. ^{1}H NMR (300 MHz, DMSO-d_6) δ 10.48 (s, 1H), 8.41 (d, *J* = 8.3 Hz, 1H), 7.99 (d, *J* = 8.3 Hz, 1H), 7.93 (s, 1H), 7.35 (d, *J* = 8.3 Hz, 1H), 5.19−5.05 (m, 1H), 4.59−4.31 (m, 1H), 4.22−3.98 (m, 2H), 3.68 (d, *J* = 15.5 Hz, 1H), 3.10 (s, 3H), 2.75−2.65 (m, 3H), 1.37 (s, 9H), 1.30−1.19 (m, 3H), 1.11 (d, *J* = 6.0 Hz, 3H). MS *m*/*z* 544 [M + Na]$^+$.

*(S)-N-((3S,4S)-7-Cyano-1-((2-methoxynaphthalen-1-yl)methyl)-4-methyl-5-(2-(methylsulfonyl)acetyl)-2-oxo-2,3,4,5-tetrahydro-1H-benzo[b][1,4]diazepin-3-yl)-2-(methylamino)propanamide Hydrochloride (**30a**). Step 1.* To a rt solution of **29** (108 mg, 207 μmol) in DMF (518 μL) was added 1-(chloromethyl)-2-methoxynaphthalene (47.1 mg, 228 μmol), cesium carbonate (81.0 mg, 248 μmol), and sodium iodide (37.2 mg, 248 μmol). The reaction was stirred at rt for 1.5 h, then diluted with EtOAc, washed with H_2O and satd aq NaCl, dried over Na_2SO_4, filtered, and concentrated. The crude material was purified by flash chromatography (12 g RediSep Gold silica gel; 40−100% EtOAc−hexanes) then preparative HPLC to provide *tert*-butyl (*S*)-1-((3*S*,4*S*)-7-cyano-1-((2-methoxynaphthalen-1-yl)methyl)-4-methyl-5-(2-(methylsulfonyl)acetyl)-2-oxo-2,3,4,5-tetrahydro-1*H*-benzo[*b*][1,4]diazepin-3-ylamino)-1-oxopropan-2-yl(methyl)-carbamate (55 mg, 38%) as a white solid. ^{1}H NMR (300 MHz, DMSO-d_6) δ 8.63 (d, *J* = 8.7 Hz, 1H), 8.13−7.81 (m, 5H), 7.57 (s, 1H), 7.47−7.30 (m, 3H), 5.91 (d, *J* = 15.1 Hz, 1H), 5.37 (d, *J* = 14.7 Hz, 1H), 4.95 (dq, *J* = 11.9, 5.9 Hz, 1H), 4.65−4.38 (m, 1H), 4.08 (dd, *J* = 11.7, 8.3 Hz, 1H), 3.86 (s, 3H), 2.87 (s, 3H), 2.73 (s, 3H), 2.10 (d, *J* = 15.1 Hz, 1H), 1.44−1.25 (m, 13H), 0.98 (d, *J* = 6.0 Hz, 3H). MS *m*/*z* 714 [M + Na]$^+$.

Step 2. A rt solution of *tert*-butyl (*S*)-1-((3*S*,4*S*)-7-cyano-1-((2-methoxynaphthalen-1-yl)methyl)-4-methyl-5-(2-(methylsulfonyl)-acetyl)-2-oxo-2,3,4,5-tetrahydro-1*H*-benzo[*b*][1,4]diazepin-3-ylamino)-1-oxopropan-2-yl(methyl)carbamate (55 mg, 79.5 μmol) in 4 M HCl in 1,4-dioxane (398 μL) was stirred for 1 h. The reaction was diluted with Et_2O and the solids were collected by vacuum filtration, taken up in MeCN−H_2O, and lyophilized to provide **30a** (41.6 mg, 83%) as a white solid. ^{1}H NMR (300 MHz, DMSO-d_6) δ 9.30 (d, *J* = 8.7 Hz, 1H), 8.89 (br s, 2H), 8.16−8.03 (m, 2H), 8.01−7.93 (m, 1H), 7.92−7.85 (m, 2H), 7.61 (d, *J* = 1.1 Hz, 1H), 7.46−7.30 (m, 3H), 5.92 (d, *J* = 14.7 Hz, 1H), 5.40 (d, *J* = 14.7 Hz, 1H), 4.86 (dq, *J* = 11.9, 6.0 Hz, 1H), 4.13 (dd, *J* = 11.7, 8.7 Hz, 1H), 3.93−3.76 (m, 4H), 2.87 (s, 3H), 2.49−2.47 (m, 3H), 2.13 (d, *J* = 15.1 Hz, 1H), 1.46 (d, *J* = 6.8 Hz, 3H), 1.36 (d, *J* = 15.1 Hz, 1H), 1.03 (d, *J* = 6.4 Hz, 3H). HRMS *m*/*z* calcd for $C_{30}H_{34}O_6N_5S$ [M + H]$^+$ 592.22243, found 592.22174.

*(S)-N-((3S,4S)-7-Cyano-4-methyl-1-((2-methylnaphthalen-1-yl)-methyl)-5-(2-(methylsulfonyl)acetyl)-2-oxo-2,3,4,5-tetrahydro-1H-benzo[b][1,4]diazepin-3-yl)-2-(methylamino)propanamide Hydrochloride (**30b**). Step 1.* To a rt solution of **29** (246 mg, 472 μmol) in DMF (1.18 mL) was added 1-(chloromethyl)-2-methylnaphthalene (98.9 mg, 519 μmol), cesium carbonate (184 mg, 566 μmol), and sodium iodide (84.8 mg, 566 μmol). The reaction was stirred at rt for 1 h. The reaction was diluted with EtOAc (60 mL), washed with H_2O (60 mL) and satd aq NaCl (60 mL), dried over Na_2SO_4, filtered, and concentrated. The crude material was purified by flash chromatography (40 g RediSep Gold silica gel; 20−100% EtOAc−hexanes) to provide *tert*-butyl (*S*)-1-((3*S*,4*S*)-7-cyano-4-methyl-1-((2-methylnaphthalen-1-yl)methyl)-5-(2-(methylsulfonyl)acetyl)-2-oxo-2,3,4,5-tetrahydro-1*H*-benzo[*b*][1,4]diazepin-3-ylamino)-1-oxopropan-2-yl(methyl)carbamate (261 mg, 82% yield) as a white solid. ^{1}H NMR (300 MHz, DMSO-d_6) δ 8.61 (d, *J* = 8.3 Hz, 1H), 8.13 (d, *J* = 8.3 Hz, 1H), 8.01−7.92 (m, 2H), 7.85 (d, *J* = 7.9 Hz, 1H), 7.72 (d, *J* = 8.3 Hz, 1H), 7.65 (s, 1H), 7.53−7.37 (m, 2H), 7.28 (d, *J* = 8.7 Hz, 1H), 5.97 (d, *J* = 15.5 Hz, 1H), 5.50 (d, *J* = 15.1 Hz, 1H), 5.04−4.91 (m, 1H), 4.62−4.41 (m, 1H), 4.05 (dd, *J* = 11.7, 8.7 Hz, 1H), 2.99 (s, 3H), 2.73 (s, 3H), 2.63 (d, *J* = 15.1 Hz, 1H), 2.46 (s, 3H), 1.92 (d, *J* = 15.1 Hz, 1H), 1.42−1.25 (m, 12H), 0.99 (d, *J* = 6.0 Hz, 3H). MS *m*/*z* 698 [M + Na]$^+$.

Step 2. A rt solution of *tert*-butyl (*S*)-1-((3*S*,4*S*)-7-cyano-4-methyl-1-((2-methylnaphthalen-1-yl)methyl)-5-(2-(methylsulfonyl)acetyl)-2-oxo-2,3,4,5-tetrahydro-1*H*-benzo[*b*][1,4]diazepin-3-ylamino)-1-oxopropan-2-yl(methyl)carbamate (260 mg, 385 μmol) in 4 M HCl in dioxane (1.92 mL) was stirred for 1 h. The reaction was added, dropwise, to a stirred vial of Et_2O (20 mL), and the solids were collected by vacuum filtration (washed with Et_2O (3 × 4 mL)). This material was taken up in MeCN−H_2O and lyophilized to provide **30b** (210 mg, 89% yield) as a white solid. ^{1}H NMR (300 MHz, DMSO-d_6) δ 9.30 (d, *J* = 8.3 Hz, 1H), 8.92 (br s, 2H), 8.12 (d, *J* = 8.3 Hz, 1H), 8.04−7.93 (m, 2H), 7.86 (d, *J* = 7.6 Hz, 1H), 7.74 (d, *J* = 8.3 Hz, 1H), 7.69 (d, *J* = 1.1 Hz, 1H), 7.54−7.37 (m, 2H), 7.29 (d, *J* = 8.3 Hz, 1H), 5.97 (d, *J* = 15.5 Hz, 1H), 5.52 (d, *J* = 15.5 Hz, 1H), 4.89 (dq, *J* = 11.9, 6.1 Hz, 1H), 4.10 (dd, *J* = 11.7, 8.7 Hz, 1H), 3.86 (q, *J* = 6.8 Hz, 1H), 3.00 (s, 3H), 2.68 (d, *J* = 15.5 Hz, 1H), 2.48 (s, 3H), 2.46 (s, 3H), 1.96 (d, *J* = 15.1 Hz, 1H), 1.47 (d, *J* = 6.8 Hz, 3H), 1.04 (d, *J* = 6.0 Hz, 3H). HRMS *m*/*z* calcd for $C_{30}H_{34}O_5N_5S$ [M + H]$^+$ 576.22752, found 576.22644.

*tert-Butyl (3S,4S)-7-Cyano-1-((2-methoxynaphthalen-1-yl)-methyl)-4-methyl-2-oxo-2,3,4,5-tetrahydro-1H-benzo[b][1,4]-diazepin-3-ylcarbamate (**31**).* To a rt solution of **27** (406 mg, 1.28 mmol) in DMF (3.21 mL) was added 1-(chloromethyl)-2-methoxynaphthalene (318 mg, 1.54 mmol) and cesium carbonate (1.25 g, 3.85 mmol). The reaction was stirred at rt for 16 h, then diluted with EtOAc, washed with H_2O and satd aq NaCl, dried over Na_2SO_4, filtered, and concentrated. The crude material was purified by flash chromatography (40 g silica gel; 0−100% EtOAc−hexanes) to provide **31** (448 mg, 72%) as an off-white solid. ^{1}H NMR (300 MHz, DMSO-d_6) δ 8.07 (d, *J* = 8.7 Hz, 1H), 7.81−7.70 (m, 2H), 7.49 (d, *J* = 8.3 Hz, 1H), 7.42−7.34 (m, 1H), 7.34−7.24 (m, 4H), 7.07 (d, *J* = 1.5 Hz, 1H), 5.82 (d, *J* = 14.7 Hz, 1H), 5.29 (d, *J* = 14.7 Hz, 1H), 4.82 (s, 1H), 3.83 (s, 3H), 3.78−3.59 (m, 2H), 1.37 (s, 9H), 0.98 (d, *J* = 5.7 Hz, 3H). MS *m*/*z* 509 [M + Na]$^+$.

*tert-Butyl (3S,4S)-5-Acetyl-7-cyano-1-((2-methoxynaphthalen-1-yl)methyl)-4-methyl-2-oxo-2,3,4,5-tetrahydro-1H-benzo[b][1,4]-diazepin-3-ylcarbamate (**32**).* To a 0 °C solution of **32** (448 mg, 921 μmol) in CH_2Cl_2 (9.21 mL) was added pyridine (375 μL, 4.6 mmol), followed by acetyl chloride (78.8 μL, 1.1 mmol) dropwise. The reaction was stirred at 0 °C for 1 h, then allowed to warm to rt and stirred for an additional 20 h, then quenched by the addition of H_2O and extracted with CH_2Cl_2. The combined organic layers were washed with satd aq $NaHCO_3$ and satd aq NaCl, dried over Na_2SO_4, filtered, and concentrated. The crude material was purified by flash chromatography (40 g silica gel; 0−100% EtOAc−hexanes) to provide **32** (316 mg, 65%) as a white solid. ^{1}H NMR (300 MHz, DMSO-d_6) δ 8.05−7.86 (m, 3H), 7.83−7.73 (m, 2H), 7.71−7.67 (m, 1H), 7.58 (d, *J* = 9.1 Hz, 1H), 7.38−7.24 (m, 3H), 5.99 (d, *J* = 14.7 Hz, 1H), 5.34 (d, *J* = 14.7 Hz, 1H), 4.82 (dq, *J* = 12.0, 6.1 Hz, 1H), 3.92−3.82 (m, 3H), 3.69 (dd, *J* = 11.9, 8.9 Hz, 1H), 1.37 (s, 9H), 0.92 (d, *J* = 6.4 Hz, 3H), 0.09 (s, 3H). MS *m*/*z* 551 [M + Na]$^+$.

*(S)-N-((3S,4S)-5-Acetyl-7-cyano-1-((2-methoxynaphthalen-1-yl)-methyl)-4-methyl-2-oxo-2,3,4,5-tetrahydro-1H-benzo[b][1,4]-diazepin-3-yl)-2-(methylamino)propanamide Hydrochloride (**33**). Step 1.* A rt solution of **32** (316 mg, 598 μmol) in 4 M HCl in 1,4-dioxane (2.99 mL) was stirred for 2 h. The reaction was diluted with Et_2O and the solids were collected by vacuum filtration to provide (3*S*,4*S*)-5-acetyl-3-amino-1-((2-methoxynaphthalen-1-yl)methyl)-4-methyl-2-oxo-2,3,4,5-tetrahydro-1*H*-benzo[*b*][1,4]diazepine-7-carbonitrile hydrochloride (216 mg, 78%) as a white solid that was used without further purification. MS *m*/*z* 429 [M + H]$^+$.

Step 2. To a 0 °C solution of (3*S*,4*S*)-5-acetyl-3-amino-1-((2-methoxynaphthalen-1-yl)methyl)-4-methyl-2-oxo-2,3,4,5-tetrahydro-1*H*-benzo[*b*][1,4]diazepine-7-carbonitrile hydrochloride (216 mg, 465 μmol) in DMF (1.55 mL) was added Boc-*N*-methyl-L-alanine (104 mg, 511 μmol), *N*,*N*-diisopropylethylamine (322 μL, 1.86 mmol), and HBTU (194 mg, 511 μmol). The reaction was stirred at rt for 30 min, then diluted with H_2O, and the solids were collected by vacuum

dx.doi.org/10.1021/jm400732v | J. Med. Chem. XXXX, XXX, XXX−XXX

filtration, taken up in EtOAc, washed with H_2O, satd aq $NaHCO_3$, and satd aq NaCl, dried over Na_2SO_4, filtered, and concentrated. The crude material was purified by flash chromatography (12 g silica gel; 20−100% EtOAc−hexanes) to provide *tert*-butyl (*S*)-1-((3*S*,4*S*)-5-acetyl-7-cyano-1-((2-methoxynaphthalen-1-yl)methyl)-4-methyl-2-oxo-2,3,4,5-tetrahydro-1*H*-benzo[*b*][1,4]diazepin-3-ylamino)-1-oxopropan-2-yl(methyl)carbamate (255 mg, 89%) as a white solid. MS *m*/*z* 636 $[M + Na]^+$.

Step 3. A rt solution of *tert*-butyl (*S*)-1-((3*S*,4*S*)-5-acetyl-7-cyano-1-((2-methoxynaphthalen-1-yl)methyl)-4-methyl-2-oxo-2,3,4,5-tetrahydro-1*H*-benzo[*b*][1,4]diazepin-3-ylamino)-1-oxopropan-2-yl(methyl)-carbamate (255 mg, 416 μmol) in 4 M HCl in 1,4-dioxane (2.08 mL) was stirred for 45 min. The reaction was diluted with Et_2O and the solids were collected by vacuum filtration, taken up in MeCN−H_2O, and lyophilized to provide **33** (181.8 mg, 80%) as a white solid. ^1H NMR (300 MHz, DMSO-d_6) δ 9.27 (d, *J* = 8.3 Hz, 1H), 8.91 (br s, 2H), 8.09−7.97 (m, 2H), 7.91 (d, *J* = 7.9 Hz, 1H), 7.84−7.72 (m, 3H), 7.40−7.25 (m, 3H), 5.99 (d, *J* = 15.1 Hz, 1H), 5.36 (d, *J* = 14.7 Hz, 1H), 4.85 (dq, *J* = 11.8, 6.0 Hz, 1H), 4.08 (dd, *J* = 11.5, 8.5 Hz, 1H), 3.94−3.78 (m, 4H), 2.48 (s, 3H), 1.47 (d, *J* = 7.2 Hz, 3H), 0.95 (d, *J* = 6.0 Hz, 3H), 0.10 (s, 3H). HRMS *m*/*z* calcd for $C_{29}H_{32}O_4N_5$ $[M + H]^+$ 514.24488, found 514.24353.

*tert-Butyl (3S,4S)-7-Cyano-4-methyl-1-((2-methylnaphthalen-1-yl)methyl)-2-oxo-2,3,4,5-tetrahydro-1H-benzo[b][1,4]diazepin-3-ylcarbamate (**34**).* To a rt solution of **27** (308 mg, 974 μmol) in DMF (2.43 mL) was added 1-(chloromethyl)-2-methylnaphthalene (223 mg, 1.17 mmol) and cesium carbonate (952 mg, 2.92 mmol). The reaction was stirred at rt for 2 h, then diluted with EtOAc, washed with H_2O and satd aq NaCl, dried over Na_2SO_4, filtered, and concentrated. The crude material was purified by flash chromatography (40 g silica gel; 0−100% EtOAc−hexanes) to provide **34** (364 mg, 80%) as an off-white oil. ^1H NMR (400 MHz, DMSO-d_6) δ 8.18 (d, *J* = 7.8 Hz, 1H), 7.79−7.73 (m, 1H), 7.65 (d, *J* = 8.6 Hz, 1H), 7.45−7.35 (m, 2H), 7.29−7.19 (m, 3H), 7.17−7.11 (m, 2H), 5.77−5.69 (m, 1H), 5.46 (d, *J* = 15.2 Hz, 1H), 4.99 (s, 1H), 3.79−3.64 (m, 2H), 2.44 (s, 3H), 1.38 (s, 9H), 1.00 (d, *J* = 5.3 Hz, 3H). MS *m*/*z* 493 $[M + Na]^+$.

*tert-Butyl (3S,4S)-5-Acetyl-7-cyano-4-methyl-1-((2-methylnaphthalen-1-yl)methyl)-2-oxo-2,3,4,5-tetrahydro-1H-benzo[b][1,4]-diazepin-3-ylcarbamate (**35**).* To a 0 °C solution of **35** (364 mg, 774 μmol) in CH_2Cl_2 (7.74 mL) was added pyridine (306 mg, 315 μL, 3.87 mmol), followed by acetyl chloride (71.8 μL, 1.01 mmol) dropwise. The reaction was stirred at 0 °C for 1 h, then allowed to warm to rt and stirred for an additional 15 h, then quenched by the addition of H_2O and extracted with CH_2Cl_2. The combined organic layers were washed with satd aq $NaHCO_3$ and satd aq NaCl, dried over Na_2SO_4, filtered, and concentrated. The crude material was purified by flash chromatography (40 g silica gel; 0−100% EtOAc−hexanes) (2×) to provide **35** (235 mg, 59%) as a white solid. ^1H NMR (400 MHz, DMSO-d_6) δ 8.09−8.03 (m, 2H), 7.91 (dd, *J* = 8.3, 1.8 Hz, 1H), 7.76 (d, *J* = 7.8 Hz, 1H), 7.73 (d, *J* = 1.8 Hz, 1H), 7.64 (d, *J* = 8.6 Hz, 1H), 7.59 (d, *J* = 8.8 Hz, 1H), 7.41 (t, *J* = 7.5 Hz, 1H), 7.35−7.28 (m, 1H), 7.20 (d, *J* = 8.3 Hz, 1H), 6.13 (d, *J* = 15.4 Hz, 1H), 5.38 (d, *J* = 15.2 Hz, 1H), 4.82 (dq, *J* = 12.1, 6.1 Hz, 1H), 3.66 (dd, *J* = 11.9, 8.8 Hz, 1H), 2.52 (s, 3H), 1.37 (s, 9H), 0.93 (d, *J* = 6.3 Hz, 3H), 0.31 (s, 3H). MS *m*/*z* 535 $[M + Na]^+$.

*(S)-N-((3S,4S)-5-Acetyl-7-cyano-4-methyl-1-((2-methylnaphthalen-1-yl)methyl)-2-oxo-2,3,4,5-tetrahydro-1H-benzo[b][1,4]-diazepin-3-yl)-2-(methylamino)propanamide Hydrochloride (**36**).* *Step 1.* A rt solution of **35** (235 mg, 458 μmol) in 4 M HCl in 1,4-dioxane (2.29 mL) was stirred for 2 h. The reaction was diluted with Et_2O and the solids were collected by vacuum filtration to provide (3*S*,4*S*)-5-acetyl-3-amino-4-methyl-1-((2-methylnaphthalen-1-yl)-methyl)-2-oxo-2,3,4,5-tetrahydro-1*H*-benzo[*b*][1,4]diazepine-7-carbonitrile hydrochloride (162 mg, 79%) as a white solid that was used without further purification. MS *m*/*z* 413 $[M + H]^+$.

Step 2. To a 0 °C solution of (3*S*,4*S*)-5-acetyl-3-amino-4-methyl-1-((2-methylnaphthalen-1-yl)methyl)-2-oxo-2,3,4,5-tetrahydro-1*H*-benzo[*b*][1,4]diazepine-7-carbonitrile hydrochloride (162 mg, 361 μmol) in DMF (1.2 mL) was added Boc-*N*-methyl-L-alanine (80.7 mg, 397 μmol), *N*,*N*-diisopropylethylamine (250 μL, 1.44 mmol), and HBTU (151 mg, 397 μmol). The reaction was stirred at rt for 30 min, then diluted with H_2O, and the solids were collected by vacuum filtration, taken up in EtOAc, washed with H_2O, satd aq $NaHCO_3$, and satd aq NaCl, dried over Na_2SO_4, filtered, and concentrated. The crude material was purified by flash chromatography (12 g silica gel; 20−100% EtOAc−hexanes) to provide *tert*-butyl (*S*)-1-((3*S*,4*S*)-5-acetyl-7-cyano-4-methyl-1-((2-methylnaphthalen-1-yl)methyl)-2-oxo-2,3,4,5-tetrahydro-1*H*-benzo[*b*][1,4]diazepin-3-ylamino)-1-oxopropan-2-yl(methyl)carbamate (189 mg, 88%) as a white solid. ^1H NMR (300 MHz, DMSO-d_6) δ 8.59 (d, *J* = 8.7 Hz, 1H), 8.11−8.02 (m, 2H), 7.94 (dd, *J* = 8.5, 1.7 Hz, 1H), 7.80−7.71 (m, 2H), 7.64 (d, *J* = 8.3 Hz, 1H), 7.42 (t, *J* = 7.4 Hz, 1H), 7.35−7.27 (m, 1H), 7.20 (d, *J* = 8.7 Hz, 1H), 6.15 (d, *J* = 15.5 Hz, 1H), 5.35 (d, *J* = 15.5 Hz, 1H), 5.00−4.85 (m, 1H), 4.69−4.36 (m, 1H), 4.00 (dd, *J* = 11.7, 8.3 Hz, 1H), 2.73 (s, 3H), 2.53 (s, 3H), 1.43−1.22 (m, 12H), 0.91 (d, *J* = 6.0 Hz, 3H), 0.30 (s, 3H). MS *m*/*z* 620 $[M + Na]^+$.

Step 3. A rt solution of *tert*-butyl (*S*)-1-((3*S*,4*S*)-5-acetyl-7-cyano-4-methyl-1-((2-methylnaphthalen-1-yl)methyl)-2-oxo-2,3,4,5-tetrahydro-1*H*-benzo[*b*][1,4]diazepin-3-ylamino)-1-oxopropan-2-yl(methyl)-carbamate (187 mg, 313 μmol) in 4 M HCl in 1,4-dioxane (1.56 mL) was stirred for 45 min. The reaction was diluted with Et_2O and the solids were collected by vacuum filtration, taken up in MeCN−H_2O, and lyophilized to provide **36** (145.5 mg, 87%) as a white solid. ^1H NMR (300 MHz, DMSO-d_6) δ 9.28 (d, *J* = 8.3 Hz, 1H), 8.93 (br s, 2H), 8.15−8.02 (m, 2H), 7.97 (dd, *J* = 8.3, 1.5 Hz, 1H), 7.83−7.74 (m, 2H), 7.66 (d, *J* = 8.3 Hz, 1H), 7.43 (t, *J* = 7.4 Hz, 1H), 7.37−7.28 (m, 1H), 7.21 (d, *J* = 8.3 Hz, 1H), 6.16 (d, *J* = 15.5 Hz, 1H), 5.37 (d, *J* = 15.5 Hz, 1H), 4.85 (dq, *J* = 12.0, 6.1 Hz, 1H), 4.05 (dd, *J* = 11.7, 8.3 Hz, 1H), 3.85 (q, *J* = 6.8 Hz, 1H), 2.53 (s, 3H), 2.48 (s, 3H), 1.48 (d, *J* = 7.2 Hz, 3H), 0.96 (d, *J* = 6.0 Hz, 3H), 0.30 (s, 3H). HRMS *m*/*z* calcd for $C_{29}H_{32}O_3N_5$ $[M + H]^+$ 498.24997, found 498.24890.

Biology. *CYP3A4 TDI Assay.* A mixture containing either 10 or 50 μM test compound, 1 mg/mL human liver microsomes, 100 mM sodium phosphate (pH 7.4), 1 mM EDTA, and 3 mM magnesium chloride was incubated at 37 °C for 10 min. The preincubation was initiated by addition of NADPH (final concentration 1 mM). Preincubations were allowed to proceed for 0.5, 2.5, 5, 10, 15, 20, 25, and 30 min. At each time point, an aliquot was taken and added to a reaction mixture containing 10 μM midazolam. This reaction was allowed to proceed for 5 min at 37 °C then terminated by the addition of an equal volume of acetonitrile. Midazolam hydroxylation was determined using LC-MS/MS. Midazolam metabolite peak areas were normalized, with 100% activity set to the reaction rate of the DMSO control at 0.5 min of preincubation time. The natural log of normalized reaction rate was plotted against preincubation time, and rate constants (k_{obs}) for loss of enzyme activity were calculated. Only points in the linear range were considered for the determination of k_{obs}. Estimation of TDI parameters, K_I and k_{inact}, were performed using Kitz−Wilson double reciprocal plots.

XIAP BIR2 and BIR3 TR-FRET Assay. Ten nanomolar of 6× histidine-tagged BIR2 (amino acids 124−240) or BIR3 (amino acids 241−356) domain of the XIAP protein was mixed with 20 nM of the peptide AVPIAQKSEK (ε-biotin)−OH 1:2 TFA in the presence of 50 mM Tris-Cl (pH 7.5), 100 mM NaCl, 1 mM dithiothreitol (DTT), and 0.1 mg/mL bovine serum albumin (BSA). Following a 45 min incubation at 37 °C, europium−streptavidin and allophycocyanin conjugated anti-histidine antibody were added to a final concentration of 1.5 nM and 15 nM, respectively. Time-resolved fluorescence resonance energy transfer (TR-FRET) signals were measured after 1 h at rt. Compound potency was assessed at 10 serially diluted concentrations. Percentage of inhibition at each concentration was determined to generate an IC_{50} value for each compound. Typically, Z' = ∼0.9.[27] A measure of the overall variability of the assay is provided by the positive control: BIR2 IC_{50} = 1.25 ± 0.91 μM (*n* = 160), BIR3 IC_{50} = 0.039 ± 0.025 μM (*n* = 168).

cIAP1 BIR2 AND BIR3 TR-FRET Assay. Thirty nanomolar of 6× histidine−thrombin−TEV tagged BIR2 (amino acids 174−256) or BIR3 (amino acids 260−352) domain of the cIAP protein was mixed with 50 nM of the peptide AVPIAQKSEK (ε-biotin)−OH 1:2 TFA in the presence of 50 mM Tris-Cl (pH 7.5), 100 mM NaCl, 1 mM

dx.doi.org/10.1021/jm400732v | J. Med. Chem. XXXX, XXX, XXX−XXX

dithiothreitol (DTT), and 0.1 mg/mL bovine serum albumin (BSA). Following a 45 min incubation at 37 °C, europium−streptavidin and allophycocyanin conjugated anti-histidine antibody were added to a final concentration of 1.5 and 15 nM, respectively. Time-resolved fluorescence resonance energy transfer (TR-FRET) signals were measured after 1 h at rt. Compound potency was assessed at 10 serially diluted concentrations. Percentage of inhibition at each concentration was determined to generate an IC_{50} value for each compound.

XIAP-Caspase Reactivation Assay. The caspase reactivation assay was performed in 20 mM HEPES buffer (pH 7.0), containing 1.5 mM $MgCl_2$, 5 mM KCl, 1 mM ethylene diamine tetraacetic acid (EDTA), 1 mM ethylene glycol tetraacetic acid (EGTA), 1 mM DTT, and 0.1 mg/mL BSA. S-100 cell extract served as the source of cellular caspases. Then 2 μM cytochrome C and 19.2 μM dATP were added to activate the caspases. The cleavage of a fluorogenic substrate specific for caspase-3 and -7, Ac-DEVD-AFC at 10 μM, was monitored at 530 nm after 4 h of incubation at rt. The addition of 0.75 nM glutathione S-transferase (GST)-tagged full length XIAP inhibited the caspase activation by ∼85%. The effect of serially diluted compounds to restore caspase activation was determined to generate an EC_{50} value for each compound.

Cell-Based Assay. SW-620 cells (1500 cells/well) were seeded into a 96 well plate one day prior to treatment. Next day, cells were treated with indicated compounds and/or antibody and further incubated at 37 °C with 5% CO_2 for 5 d. Cell Titer 96 Aqueous One solution (25 μL/well, Promega cat. no. G3580) was added, and the plates were further incubated for 2−3 h. Plates OD at 490 nm was determined using Envision 2101 plate reader (PerkinElmer), and EC_{50} values were determined for compounds or antibody.

TNFα ELISA Assay. MDA-231 cells (400000 cells/well) were seeded into 24 well plates and incubated for 24 h. Next day, media was aspirated from wells and replaced with either compound or media alone (400 μL/well) and further incubated at 37 °C with 5% CO_2 for an additional 19 h. Total media volume was then collected and centrifuged (1000g) at 4 °C to pellet debris. TNF of media was quantitated by ELISA (TNF Human ELISA kit, R&D Systems cat. no. DTA00B) and results plotted following subtraction of background values (media, no cells).

LOX Xenograft PD Study. The study was carried out with LOX xenografts in female nude mice (d 15). A single dose of compound was administered as follows: conatumumab 1 mg/kg ip, **3** 100 mg/kg po, **36**, and 200 mg/kg po. Xenografts were removed 8 h postdose, frozen (−80 °C), transferred to 15 mL conical tubes on dry ice, and treated with 1× lysis buffer (20 mM Tris-HCl (pH 7.5), 150 mM NaCl, 1 mM EDTA, 1 mM EGTA, 1% TX-100, 5 mM sodium pyrophosphate, 1 mM β-glycerophosphate, 10 mM sodium fluoride, 1 mM Na_3VO_4, and 1 mM benzamidine. EMD proteinase inhibitor cocktail V) (1 mL per ∼0.1 g (if tumor is big >0.4, add 1 mL/0.2 g). Tumors were homogenized at full speed, diluted with the same volume of lysis buffer, and kept on ice for 20 min. A portion of the homogenate (2 mL) was transferred to a microcentrifuge tube and thawed at full speed for 20 min at 4 °C. The supernatant was optionally centrifuged again. Protein was quantitated and samples were prepared for caspase assay and Western blot analysis (50 μg of total protein was used for caspase assay/60 μg of total protein was used for Western blot). Tumor lysate (10 μL, 5 μg/μL) was added into white solid 96 well plate. Caspase-3/7 assay buffer (final concentration: 10 mM Tris, 5 mM DTT, 1 mM EDTA, 50 μM DEVD-AMC, 20 mM NaCl, 1% NP-40) (90 μL) was added into each well. The plate was incubated for 2 h at rt with shaking and read at 385/460 nM.

■ ASSOCIATED CONTENT

Supporting Information

Full procedures for compounds **7** through **26a−f**, crystallographic method, data collection, and refinement statistics. This material is available free of charge via the Internet at http://pubs.acs.org.

Accession Codes

The PDB ID code for **21j** bound to XIAP BIR2 shown in Figure 3 is 4KJU.

■ AUTHOR INFORMATION

Corresponding Author

*E-mail: rfkester@yahoo.com. Phone: 973-498-8986.

Author Contributions

All authors have given approval to the final version of the manuscript.

Notes

The authors declare no competing financial interest.

■ ACKNOWLEDGMENTS

We thank Dr. Pamela Carroll and Dr. David Heimbrook for their helpful discussions and support, Charles Belunis for protein purification, Santina Russo and Joachim Diez of Expose for data collection at SLS, and Kuresh Youdim and Volkmar Starke for providing support for the TDI assay.

■ ABBREVIATIONS USED

IAPs, inhibitor of apoptosis proteins; XIAP, X-linked inhibitor of apoptosis protein; cIAP, cellular inhibitor of apoptosis protein; BIR, baculovirus IAP repeat domains; TNFα, tumor necrosis factor alpha; Smac, second mitochondria-derived activator of caspases; DIABLO, direct IAP-binding protein with low p*I*; TDI, time dependent inhibition; ATP, adenosine triphosphate; PD, pharmacodynamic; RING, really interesting new gene; TRAIL, TNF-related apoptosis-inducing ligand; HBPyU, *O*-(benzotriazol-1-yl)-*N*,*N*,*N*′,*N*′-bis(tetramethylene)-uronium hexafluorophosphate; EDCI, *N*-(3-dimethylaminopropyl)-*N*′-ethylcarbodiimide hydrochloride; HOBt, hydroxybenzotriazole; HBTU, *O*-(benzotriazol-1-yl)-*N*,*N*,*N*′,*N*′-tetramethyluronium hexafluorophosphate

■ REFERENCES

(1) Hanahan, D.; Weinberg, R. A. Hallmarks of Cancer: The Next Generation. *Cell* **2011**, *144*, 646−674.

(2) Salvesen, G. S.; Abrams, J. M. Caspase activation—stepping on the gas or releasing the brakes? Lessons from humans and flies. *Oncogene* **2004**, *23*, 2774−2784.

(3) (a) Tamm, I.; Richter, S.; Oltersdorf, D.; Creutzig, U.; Harbott, J.; Scholz, F.; Karawajew, L.; Ludwig, W.-D.; Wuchter, C. High Expression Levels of X-Linked Inhibitor of Apoptosis Protein and Survivin Correlate with Poor Overall Survival in Childhood de Novo Acute Myeloid Leukemia. *Clin. Cancer Res.* **2004**, *10*, 3737−3744. (b) Tamm, I.; Richter, S.; Scholz, F.; Schmelz, K.; Oltersdorf, D.; Karawajew, L.; Schoch, D.; Haferlach, T.; Ludwig, W. D.; Wuchter, C. XIAP expression correlates with monocytic differentiation in adult de novo AML: impact on prognosis. *Hematol. J.* **2004**, *5*, 489−495.

(4) Kluger, H. M.; McCarthy, M. M.; Alvero, A. B.; Sznol, M.; Ariyan, S.; Camp, R. L.; Rimm, D. L.; Mor, G. The X-linked inhibitor of apoptosis protein (XIAP) is up-regulated in metastatic melanoma, and XIAP cleavage by phenoxodiol is associated with carboplatin sensitization. *J. Transl. Med.* **2007**, *5*, 6.

(5) Mizutani, Y.; Nakanishi, H.; Li, Y. N.; Matsubara, H.; Yamamoto, K.; Sato, N.; Shiraishi, T.; Nakamura, T.; Mikami, K.; Okihara, K.; Takaha, N.; Ukimura, O.; Kawauchi, A.; Nonomura, N.; Bonavida, B.; Miki, T. Overexpression of XIAP expression in renal cell carcinoma predicts a worse prognosis. *Int. J. Oncol.* **2007**, *30*, 919−925.

(6) Miller, L. K. An exegesis of IAPs: salvation and surprises from BIR motifs. *Trends Cell Biol.* **1999**, *9*, 323−328.

(7) Jiang, X.; Wang, X. Cytochrome C-Mediated Apoptosis. *Annu. Rev. Biochem.* **2004**, *73*, 87−106.

(8) Ashkenazi, A.; Dixit, V. M. Death Receptors: Signaling and Modulation. *Science* **1998**, *281*, 1305−1308.
(9) Fuentes-Prior, P.; Salvesen, G. S. The protein structures that shape caspase activity, specificity, activation and inhibition. *Biochem. J.* **2004**, *384*, 201−232.
(10) Eckelman, B. P.; Salvesen, G. S.; Scott, F. L. Human inhibitor of apoptosis proteins: why XIAP is the black sheep of the family. *EMBO Rep.* **2006**, *7*, 988−994.
(11) (a) Du, C.; Fang, M.; Li, Y.; Li, L.; Wang, X. Smac, a Mitochondrial Protein that Promotes Cytochrome c-Dependent Caspase Activation by Eliminating IAP Inhibition. *Cell* **2000**, *102*, 33−42. (b) Verhagen, A. M.; Ekert, P. G.; Pakusch, M.; Silke, J.; Connolly, L. M.; Reid, G. E.; Moritz, R. L.; Simpson, R. J.; Vaux, D. L. Identification of DIABLO, a Mammalian Protein that Promotes Apoptosis by Binding to and Antagonizing IAP Proteins. *Cell* **2000**, *102*, 43−53.
(12) (a) Wu, G.; Chai, J.; Suber, T. L.; Wu, J.-W.; Du, C.; Wang, X.; Shi, Y. Structural basis of IAP recognition by Smac/DIABLO. *Nature* **2000**, *408*, 1008−1012. (b) Liu, Z.; Sun, C.; Olejniczak, E. T.; Meadows, R. P.; Betz, S. F.; Oost, T.; Herrmann, J.; Wu, J. C.; Fesik, S. W. Structural basis for binding of Smac/DIABLO to the XIAP BIR3 domain. *Nature* **2000**, *408*, 1004−1008.
(13) In addition to the molecules specifically mentioned in this paper, other monovalent XIAP inhibitors have been reported, as well as bivalent inhibitors such as AEG40826/HGS1029, which has also entered the clinic. For further discussion, see ref 17.
(14) Cai, Q.; Sun, H.; Peng, Y.; Lu, J.; Nikolovska-Coleska, Z.; McEachern, D.; Liu, L.; Qiu, S.; Yang, C.-Y.; Miller, R.; Yi, H.; Zhang, T.; Sun, D.; Kang, S.; Guo, M.; Leopold, L.; Yang, D.; Wang, S. A Potent and Orally Active Antagonist (SM-406/AT-406) of Multiple Inhibitor of Apoptosis Proteins (IAPs) in Clinical Development for Cancer Treatment. *J. Med. Chem.* **2011**, *54*, 2714−2726.
(15) Flygare, J. A.; Beresini, M.; Budha, N.; Chan, H.; Chan, I. T.; Cheeti, S.; Cohen, F.; Deshayes, K.; Doerner, K.; Eckhardt, S. G.; Elliott, L. O.; Feng, B.; Franklin, M. C.; Reisner, S. F.; Gazzard, L.; Halladay, J.; Hymowitz, S. G.; La, H.; LoRusso, P.; Maurer, B.; Murray, L.; Plise, E.; Quan, C.; Stephan, J.-P.; Young, S. G.; Tom, J.; Tsui, V.; Um, J.; Varfolomeev, E.; Vucic, D.; Wagner, A. J.; Wallweber, H. J. A.; Wang, L.; Ware, J.; Wen, Z.; Wong, H.; Wong, J. M.; Wong, M.; Wong, S.; Yu, R.; Zobel, K.; Fairbrother, W. J. Discovery of a Potent Small-Molecule Antagonist of Inhibitor of Apoptosis (IAP) Proteins and Clinical Candidate for the Treatment of Cancer (GDC-0152). *J. Med. Chem.* **2012**, *55*, 4101−4113.
(16) (a) Houghton, P. J.; Kang, M. H.; Reynolds, C. P.; Morton, C. L.; Kolb, E. A.; Gorlick, R.; Keir, S. T.; Carol, H.; Lock, R.; Maris, J. M.; Billups, C. A.; Smith, M. A. Initial Testing (Stage 1) of LCL161, a SMAC Mimetic, by the Pediatric Preclinical Testing Program. *Pediatr. Blood Cancer* **2012**, *58*, 636−639. (b) Chen, K.-F.; Lin, J.-P.; Shiau, C.-W.; Tai, W.-T.; Liu, C.-Y.; Yu, H.-C.; Chen, P.-J.; Cheng, A.-L. Inhibition of Bcl-2 improves effect of LCL 161, a SMAC, mimetic in hepatocellular carcinoma cells. *Biochem. Pharmacol.* **2012**, *84*, 268−277.
(17) Fulda, S.; Vucic, D. Targeting IAP proteins for therapeutic intervention in cancer. *Nature Rev. Drug Discovery* **2012**, *11*, 109−123.
(18) Wu, H.; Tschopp, J.; Lin, S.-C. Smac Mimetics and TNFα: A Dangerous Liaison? *Cell* **2007**, *131*, 655−658.
(19) Gonzalez-Lopez, M.; Welsh, K.; Finlay, D.; Ardecky, R. J.; Ganji, S. R.; Su, Y.; Yuan, H.; Teriete, P.; Mace, P. D.; Riedl, S. J.; Vuori, K.; Reed, J. C.; Cosford, N. D. P. Design, synthesis and evaluation of monovalent Smac mimetics that bind to the BIR2 domain of the anti-apoptotic protein XIAP. *Bioorg. Med. Chem. Lett.* **2011**, *21*, 4332−4336.
(20) Donnell, A. F.; Michoud, C.; Rupert, K. C., Han, X.; Aguilar, D.; Frank, K. B.; Fretland, A. J.; Gao, L.; Goggin, B.; Hogg, J. H.; Hong, K.; Janson, C. A.; Kester, R. F.; Kong, N.; Le, K.; Li, S.; Liang, W.; Lombardo, L. J.; Lou, Y.; Lukacs, C.; Mischke, S.; Moliterni, J. A. ; Polonskaia, A.; Schutt, A. D.; Solis, D. S.; Specian, A.; Taylor, R. T.; Weisel, M.; Remiszewski, S. W. Benzazepinones and Benzoxazepinones as Antagonists of Inhibitor of Apoptosis Proteins (IAPs) Selective for the Second Baculovirus IAP Repeat (BIR2) Domain. *J. Med. Chem.* **2013**, DOI 10.1021/jm400731m.
(21) Schutt, A.; Goggin, B. S.; Hong, K.; Polonskaia, A.; To, T.; Tardell, C.; Dvorozniak, M.; Tannu, S.; Aguilar, D.; Solis, D.; Gao, L.; Lukacs, C.; Jansen, G.; Hilton, H.; Fretland, A.; Liang, Z.; Lee, K.; Kester, R.; Donnell, A.; Mischke, S.; Han, X.; Chen, S.; Le, N.; Lou, Y.; Remiszewski, S.; Packman, K.; Lee, E. C. Unpublished results.
(22) Lauffer, D. J.; Mullican, M. D. A Practical Synthesis of (*S*) 3-*tert*-Butoxycarbonylamino-2-oxo-2,3,4,5-tetrahydro-1,5-benzodiazepine-1-acetic Acid Methyl Ester as a Conformationally Restricted Dipeptido-Mimetic for Caspase-1 (ICE) Inhibitors. *Bioorg. Med. Chem. Lett.* **2002**, *12*, 1225−1227.
(23) Lukacs, C. M.; Belunis, C.; Crowhter, R.; Danho, W.; Gao, L.; Goggin, B.; Janson, C. A.; Li, S.; Remiszewski, S.; Schutt, A.; Thakur, M. K.; Singh, S. K.; Swaminathan, S.; Pandey, R.; Tyagi, R.; Gosu, R.; Kamath, A. V.; Kuglstatter, A. The Crystal Structure of XIAP-BIR2: Understanding selectivity of the BIR domains. *Acta Crystallogr., Sect. D.: Biol. Crystallogr.* **2013**, *69*, 1717−1725.
(24) Dobler, M. R.; Lenoir, F.; Parker, D. T.; Peng, Y.; Piizzi, G.; Wattanasin, S. Organic Compounds for Application in Bacterial Infection Treatment. PCT International Application PCT/EP2009/061905, 2009.
(25) Chen, Y.; Liu, L.; Monshouwer, M.; Fretland, A. J. Determination of Time-Dependent Inactivation of CYP3A4 in Cryopreserved Human Hepatocyctes and Assessment of Human Drug-Drug Interactions. *Drug Metab. Dispos.* **2011**, *39*, 2085−2092.
(26) Gaither, A.; Porter, D.; Yao, Y.; Borawski, J.; Yang, G.; Donovan, J.; Sage, D.; Slisz, J.; Tran, M.; Straub, C.; Ramsey, T.; Iourgenko, V.; Huang, A.; Chen, Y.; Schlegel, R.; Labow, M.; Fawell, S.; Sellers, W. R.; Zawel, L. A Smac Mimetic Rescue Screen Reveals Roles for Inhibitor of Apoptosis Proteins in Tumor Necrosis Factor-α Signaling. *Cancer Res.* **2007**, *67*, 11493−11498.
(27) Zhang, J.-H.; Chung, T. D. Y.; Oldenburg, K. R. A Simple Statistical Parameter for Use in Evaluation and Validation of High Throughput Screening Assays. *J. Biomol. Screening* **1999**, *4*, 67−73.